


Problems of Identification and Quantification in Archaeozoological Analysis, Part II: Presentation of an Alternative Counting Method

Eugène Morin^{1,2}  · Elspeth Ready³ ·
Arianne Boileau⁴ · Cédric Beauval⁵ ·
Marie-Pierre Coumont⁶

Published online: 26 September 2016
© Springer Science+Business Media New York 2016

Abstract Archaeozoologists commonly use Number of Identified SPecimens (NISP) and Minimum Number of Elements (MNE) as measures of anatomical abundances. According to a blind test examining the reproducibility and accuracy of identifications of ungulate remains (Morin *et al.*, Part I, Journal of Archaeological Method and Theory, doi: 10.1007/s10816-016-9300-4), NISP provides estimates of skeletal abundances that are less robust than those based on MNE. However, although results were improved with the latter method, MNE is not free of problems. Here, we show through an analysis of paired NISP-MNE data for 24 classes of elements that MNE is prone to inflate the representation of rare parts (as measured by NISP), a phenomenon more strongly expressed in certain elements than in others. Moreover, some elements show a wide scatter of points, which raises issues of data reproducibility. MNE is also known

Electronic supplementary material The online version of this article (doi:10.1007/s10816-016-9301-3) contains supplementary material, which is available to authorized users.

✉ Eugène Morin
eugenemorin@trentu.ca

¹ Department of Anthropology, DNA Block C, Trent University, 2140 East Bank Drive, Peterborough, ON K9J 7B8, Canada

² PACEA, Bâtiment B18, UMR5199, Université de Bordeaux, Allée Geoffroy St-Hilaire CS50023, 33615 Pessac CEDEX, France

³ Department of Anthropology, Stanford University, Main Quad Building 50, 450 Serra Mall, Stanford, CA 94305-2034, USA

⁴ Department of Anthropology, University of Florida, Turlington Hall, Room 1112, PO Box 117305, Gainesville, FL 32611, USA

⁵ Archéosphère, 2 rue des noyers, 11500 Quirbajou, France

⁶ ANRAS, CEF La Poujade, Limayrac, 12240 Colombiès, France

for being seriously affected by aggregation methods. These fundamental problems severely undermine the value of MNE as a measure of abundance. This article introduces an alternative counting method that avoids many of the weaknesses of MNE. This counting method, called the Number of Distinct Elements (NDE), focuses on the occurrence of pre-determined, invariant landmarks counted on mutually exclusive specimens. Preliminary experimental results suggest that NDE counts are robust predictors of skeletal, and perhaps taxonomic, abundances. Moreover, the NDE approach eliminates the complex and time-consuming task of spreading or drawing specimens to identify fragment overlap. Furthermore, NDE values are additive and easy to calculate. Given these features, the NDE approach represents a compelling alternative to MNE in archaeozoological analysis.

Keywords Archaeology · Faunal analysis · Blind test · Bone identification · Archaeozoology

Introduction

In part I of this contribution, the reproducibility and accuracy of Number of Identified SPecimens (NISP), Minimum Number of Elements (MNE), and, to a lesser extent, Minimum Number of Individuals (MNI) tallies were assessed in a blind test focused on problems in the identification and quantification of ungulate remains. Analysis of experimental data showed that MNE counts give more robust estimates of skeletal abundances than NISP. Given these results, one might conclude that MNE should be widely adopted. However, several points make this conclusion premature. One of these points concerns the behavior of MNE with respect to sample size, an issue that could not be investigated in the blind test. In this paper, we examine how NISP and MNE are numerically related in a large sample of assemblages and review the implications of this relationship for the analysis of skeletal abundances.

A small number of studies have previously investigated the relationship between NISP and MNE. Grayson and Frey (2004) observed strong correlations ($r \geq 0.90$, $p > 0.001$) between paired NISP-MNE data in three Paleolithic collections, which was interpreted as indicating that the two measures may frequently yield consistent results. Lyman (2008) reached a similar conclusion after studying 29 assemblages, although his analysis documented a wider spread of correlation coefficients ($r = 0.66\text{--}0.96$). These authors noted that these correlations are not surprising given that MNE counts are ultimately derived from NISP counts. In fact, the question asked here is one of sampling. Are MNE values reflecting the underlying structure of the NISP sample? In other words, can MNE values be treated as a random, and therefore representative, sample of NISP values? Because MNE is closely linked in its construction to the more intensively studied MNI, it seems legitimate to ask whether they are affected by the same sampling problems. A short discussion of MNI helps to clarify this point.

Ducos (1968) should be credited for having first demonstrated the tendency for MNI to increase according to a power function as NISP gets larger. He showed that the net effect of this trend is that MNI inflates the representation of taxa with low NISP counts in archaeological collections, particularly at small sample sizes. As noted by Grayson

(1984) and Lyman (2008), the reason for this inflation is easily understood. The first fragment attributed to a new taxon automatically entails the presence of one individual of that taxon in the sample. However, the probability of assigning a second fragment from the same taxon to a second individual is smaller than one because the specimen may derive from the previously identified individual. The probability that a third fragment will represent a new individual is even lower as that specimen may belong to the first, a second, or even a third individual. As a result of the decreasing probability of identifying a new individual, MNI *has* to be curvilinearly related to NISP in fragmented assemblages. There is ample evidence that this is indeed the case, at least in small samples (Ducos 1968; Casteel 1977; Grayson 1978a, b, 1984; Lyman 2008; Cannon 2013).

Because the identification of distinct elements proceeds in a similar fashion and provides the foundations for the derivation of MNI values, MNE should likewise artificially inflate the representation of rare parts as measured by NISP. This problem deserves serious consideration because it implies that MNE values may tally specimens in a fundamentally different way in samples that differ appreciably in NISP size and/or patterns of skeletal representation. In this paper, we evaluate this hypothesis using paired NISP-MNE data from archaeological assemblages. The analysis of these data is followed by an examination of an alternative metric of abundance that circumvents most of the problems encountered with MNE and MNI.

Materials and Methods

To assess whether MNE tends to inflate the representation of elements with low NISP counts, we compiled paired NISP-MNE data for 58 Western European assemblages excavated and analyzed according to modern standards. These assemblages, which are characterized by a wide spectrum of NISP sample sizes (25–18,523; Table 1), are all of Pleistocene age and derive from cave, rockshelter, or cliff deposits. The faunal remains were, in each case, primarily accumulated by humans, although carnivore intervention is sometimes also documented (*e.g.*, Teixoneres cave level III, Rosell *et al.* 2010). To control for taxonomic differences in skeletal morphology, only two closely related species are considered in the dataset: red deer (*Cervus elaphus*) and reindeer (*Rangifer tarandus*).

Although comparing the overall relationship between NISP-MNE relationships across assemblages is an approach that has previously proven productive (Grayson and Frey 2004; Lyman 2008), the present study examines relationships *within classes of skeletal parts* to assess the impact of calculation methods at the anatomical level. This means that each NISP-MNE relationship focuses on a single class of elements (*e.g.*, the mandible) with each data point in the scatter plots representing that element in a different assemblage. Correlations were calculated for 24 classes of skeletal elements, including the cranium; mandible; hyoid; all main types of vertebrae (atlas, axis, other cervical vertebrae, thoracic vertebrae, lumbar vertebrae, sacrum); scapula; ribs; innominates; all six types of long bones; malleolus; carpals; tarsals; and phalanges. NISP-MNE relationships were analyzed by comparing coefficients of determination (R^2) obtained using a linear versus power function. In these comparisons, a better fit with a power

Table 1 Archaeological red deer (*Cervus elaphus*) and reindeer (*Rangifer tarandus*) samples used in the analysis of the relationship between NISP and MNE

Assemblage, layer (period)	Taxon	NISP	Reference
Lazaret, UA25 (Ach)	Cel	993	Valensi et al. 2013, p. 130
Gran Dolina, T10-1 (Ach/MP)	Cel	468	Blasco 2011, p. 179
Abri Moula, XV (MP)	Cel	59	Valensi et al. 2012, p. 50
Arma delle Manie (MP)	Cel	794	Psathi 2003, p. 526 (“adultes” count)
Cova Bolomor, IV (MP)	Cel	385	Blasco 2011, p. 507
”, XI (MP)	Cel	39	”, p. 436
”, XVIIa (early MP)	Cel	130	”, p. 377
”, XVIIc (early MP)	Cel	91	”, p. 314
Fumane, A9 (MP)	Cel	427	Romandini et al. 2014, p. 22–23
Les Fieux, G5-G6 Total (MP)	Cel	71	Gerbe 2010, p. 397
”, G7 (MP)	Cel	66	”, p. 335
”, I-J (MP)	Cel	205	”, p. 343
Teixoneres, III (MP)	Cel	25	Rosell et al. 2010, p. 143
El Miron, 106 (UP)	Cel	124	Marín Arroyo 2009, p. 85
”, 107.2 (UP)	Cel	119	”
”, 108 (UP)	Cel	914	”
Picareiro, F (UP)	Cel	123	Haws 2003, p. 194
Riparo Dalmeri, 26c (UP)	Cel	119	Fiore and Tagliacozzo 2008, pp. 217–218, 220
Tournal, H (UP)	Cel	48	Magniez 2010, Annexe A
Abri Romani, Ja (MP)	cervids	297	Rosell 2001, p. 213
”, K (MP)	cervids	260	Fernández-Laso 2010, p. 152
”, M (MP)	cervids	346	”, p. 411
La Quina Amont, 7 (MP) ^a	Rang	196	Chase 1999, pp. 167, 170
”, 8 (MP)	Rang	995	”
Jonzac, 22 (MP)	Rang	1687	Niven et al. 2012, p. 631
Saint-Césaire, EJOP sup (MP/UP)	Rang	144	Morin 2012, pp. 281–282
”, EJOP inf (MP)	Rang	88	”, pp. 279–280
”, EGPF (MP)	Rang	198	”, pp. 277–278
Abri Pataud, 2 (UP) ^b	Rang	1650	Cho 1998, pp. 453–455, 508
”, 3 ens. 1 (UP)	Rang	991	”, pp. 457, 464–465
”, 3 ens. 2 (UP)	Rang	626	”, pp. 458, 466–467
”, 3 ens. 3 (UP)	Rang	3317	”, pp. 459, 468–469
”, 3 ens. 4 (UP)	Rang	485	”, pp. 460, 470–471
”, éboulis 3–4 (UP)	Rang	3950	”, pp. 474, 478–479, 510
”, 4-upper (UP)	Rang	18,523	”, pp. 487, 492–493
”, 4-middle (UP)	Rang	9137	”, pp. 488, 494–495
”, 4-lower (UP)	Rang	5673	”, pp. 489, 496–497
Castanet (UP)	Rang	932	Castel 2011, p. 803
Combe Saunière, IV (UP)	Rang	3079	Castel 1999, p. 232, Table XII-3
Enval 2 (UP)	Rang	46	Surmély et al. 1997, p. 179

Table 1 (continued)

Assemblage, layer (period)	Taxon	NISP	Reference
Grotte du Bison, D (UP)	Rang	176	David et al. 2005, p. 37
Grotte du Renne, VII (UP)	Rang	1259	David and Poulain 2002, p. 68
”, Xc (UP)	Rang	801	Tolmie 2013, pp. 126–127, 130–131, 141
Isturitz, Auri. ancien (UP)	Rang	374	Soulier 2013, Annexe p. 32
”, Auri. intermédiaire (UP)	Rang	45	”, p. 31
”, Protoaurignacien (UP)	Rang	68	”, p. 30
La Plaine (UP)	Rang	274	Kuntz 2006, pp. 158, 161
La Quina Aval, Auri. anc. (UP)	Rang	2353	Soulier 2013, Annexe p. 25
Le Flageolet, V (UP)	Rang	1496	Enloe 1993, p. 108
Moulin-Neuf (UP)	Rang	105	Costamagno 1999, Table 10–83
Saint-Césaire, EJJ (UP)	Rang	214	Morin 2012, pp. 295–296
”, EJM (UP)	Rang	551	”, pp. 293–294
”, EJF (UP)	Rang	2702	”, pp. 291–292
”, EJO sup (UP)	Rang	324	”, pp. 287–288
Rond-du-Barry, E (UP)	Rang	197	Costamagno 1999:Table 10–105
”, F2 (UP)	Rang	384	”, Tables 10–104
Tournal, H (UP)	Rang	2910	Magniez 2010, Annexe A
”, G (UP)	Rang	5343	”, Annexe A

Assemblages are listed in alphabetical order by taxon and cultural period, and within sites, from latest to earliest. Samples labeled “cervids” are largely, if not exclusively, dominated by red deer. The NISP values in the third column are those for the sum of elements included in our analysis; these values are generally smaller than the published NISP for the same taxon. The raw data and notes associated with these data can be consulted in the SOM, Table 1. Counts for the cranium and mandible were ignored when isolated teeth were not identified as deriving from the upper or lower jaw. For long bones, we summed NISP data for all long bone regions. Ulna counts were included with radius counts. For Castanet and La Quina Amont, only data for long bones were available or could be derived. Values were ignored when reported for anatomical units larger than those examined here (e.g., “all tarsals” or “carpals/tarsals”). When there was disagreement between tables, the largest NISP or MNE value was used

Ach Acheulean, *MP* Middle Paleolithic, *UP* Upper Paleolithic, *Cel* *Cervus elaphus*, *Rang* *Rangifer tarandus*

^a The MNE data for La Quina Amont are estimations based on graphs

^b Concerning Abri Pataud, although MNE data are available for phalanges, these tallies were ignored because they were apparently not derived in a standard way (our reconstructed counts suggest that they simply correspond to the sum of the left and right MNIs for the combined phalanges rather than for all three types of phalanges)

function means that the two measures increase at different rates with increasing sample size. This last pattern is problematic because it implies that the two metrics will not be fully comparable at different sample sizes and depending on methods of aggregation (Grayson 1984). We also note that some variation, due to differences in patterns of site occupation, context of preservation, and degree of fragmentation, is expected in the dataset. Nonetheless, the fact that the same assemblages—or a sub-sample of these assemblages in cases of missing data—are included in the regressions should make the results roughly comparable between classes of elements.

Analysis of the NISP-MNE Data

Table 2 gives the regression equations obtained for each of the 24 classes of skeletal elements. When all the assemblages with relevant data are considered, the comparisons indicate that a linear function provides the best-fit model in 13 classes of elements, whereas a power function gives the most parsimonious model for 8 classes of elements. These differences in frequencies are not statistically different from random ($\chi^2 = 1.2$, $p = 0.28$). Best-fit models are shown for the long bones in Fig. 1. We note that for some elements, the power function substantially improves the strength of the NISP-MNE relationship, as is the case for ribs (linear: $R^2 = 0.58$, $p < 0.0001$; power: $R^2 = 0.74$, $p < 0.0001$), cervical vertebrae other than the atlas or axis (linear: $R^2 = 0.59$, $p < 0.0001$; power: $R^2 = 0.88$, $p < 0.0001$) and thoracic vertebrae (linear: $R^2 = 0.61$, $p < 0.0001$; power: $R^2 = 0.79$, $p < 0.0001$).

Table 2 Best-fit relationships between NISP and MNE data for a sample of Paleolithic assemblages

	Linear Function		Power Function	
	R^2	equation	R^2	equation
long bones				
humerus (n=57)	0.98	$y = 0.1551x + 4.7846$	0.92	$y = 0.8063x^{0.7289}$
radio-ulna (n=57)	0.70	$y = 0.0455x + 9.1355$	0.90	$y = 0.9808x^{0.6031}$
metacarpal (n=55)	0.71	$y = 0.0817x + 7.4522$	0.89	$y = 0.6495x^{0.7147}$
femur (n=57)	0.98	$y = 0.1575x + 2.5794$	0.90	$y = 0.7990x^{0.7030}$
tibia (n=58)	0.95	$y = 0.0826x + 11.0602$	0.92	$y = 0.7761x^{0.7053}$
metatarsal (n=58)	0.96	$y = 0.0823x + 6.4061$	0.87	$y = 0.5781x^{0.7098}$
large non-lbn				
cranium (n=33)	0.76	$y = 0.115x + 0.9618$	0.71	$y = 0.7899x^{0.5386}$
mandible (n=33)	0.82	$y = 0.1091x + 4.0975$	0.76	$y = 0.9293x^{0.608}$
scapula (n=47)	0.77	$y = 0.1799x + 1.7717$	0.89	$y = 0.8712x^{0.6472}$
rib (n=31)	0.58	$y = 0.0834x + 4.376$	0.74	$y = 0.8123x^{0.6111}$
innominates (n=43)	0.73	$y = 0.1594x + 2.1767$	0.86	$y = 1.0602x^{0.5884}$
vertebrae				
atlas (n=14)	0.89	$y = 0.7599x + 0.1633$	0.88	$y = 0.9436x^{0.8642}$
axis (n=11)	0.94	$y = 0.7405x + 0.4016$	0.86	$y = 0.9574x^{0.9}$
other cerv. (n=18)	0.59	$y = 0.2755x + 1.4955$	0.88	$y = 1.0453x^{0.6457}$
thoracic (n=22)	0.61	$y = 0.2617x + 1.7995$	0.79	$y = 0.8974x^{0.6925}$
lumbar (n=22)	0.92	$y = 0.3484x + 0.1825$	0.88	$y = 0.8154x^{0.7125}$
sacrum (n=11)	0.88	$y = 0.6282x + 0.4349$	0.94	$y = 1.0007x^{0.8038}$
small/short bones				
hyoid (n=9)	0.83, $p=0.0001$	$y = 0.326x + 0.8745$	0.76, $p<.01$	$y = 1.0118x^{0.6086}$
carpals (n=41)	0.99	$y = 0.9776x - 1.5564$	0.91	$y = 0.9258x^{0.9549}$
malleolus (n=19)	1.00	$y = 0.9746x + 0.1255$	1.00	$y = 1.003x^{0.9958}$
talus (n=29)	0.99	$y = 0.9206x - 0.436$	0.99	$y = 1.0034x^{0.9449}$
calcaneus (n=33)	0.99	$y = 0.6287x + 0.722$	0.97	$y = 0.9703x^{0.8856}$
other tarsals (n=29)	1.00	$y = 0.9277x - 0.3508$	0.96	$y = 0.9501x^{0.9644}$
phalanges (n=43)	0.98	$y = 0.708x - 0.7799$	0.98	$y = 0.9379x^{0.927}$

The number of assemblages that could be included in the regression analysis is given in parentheses in the leftmost column. A gray background identifies the relationship with the highest coefficient of determination (R^2) for a given skeletal element. All results are significant at <0.0001 except when specified otherwise. Within a class of elements, NISP counts were combined for all bone regions, whereas the MNE value was derived from the best represented bone portion. In case of conflicting counts, the highest NISP or MNE value reported was used in the calculations. The raw data can be consulted in the SOM, Table 1

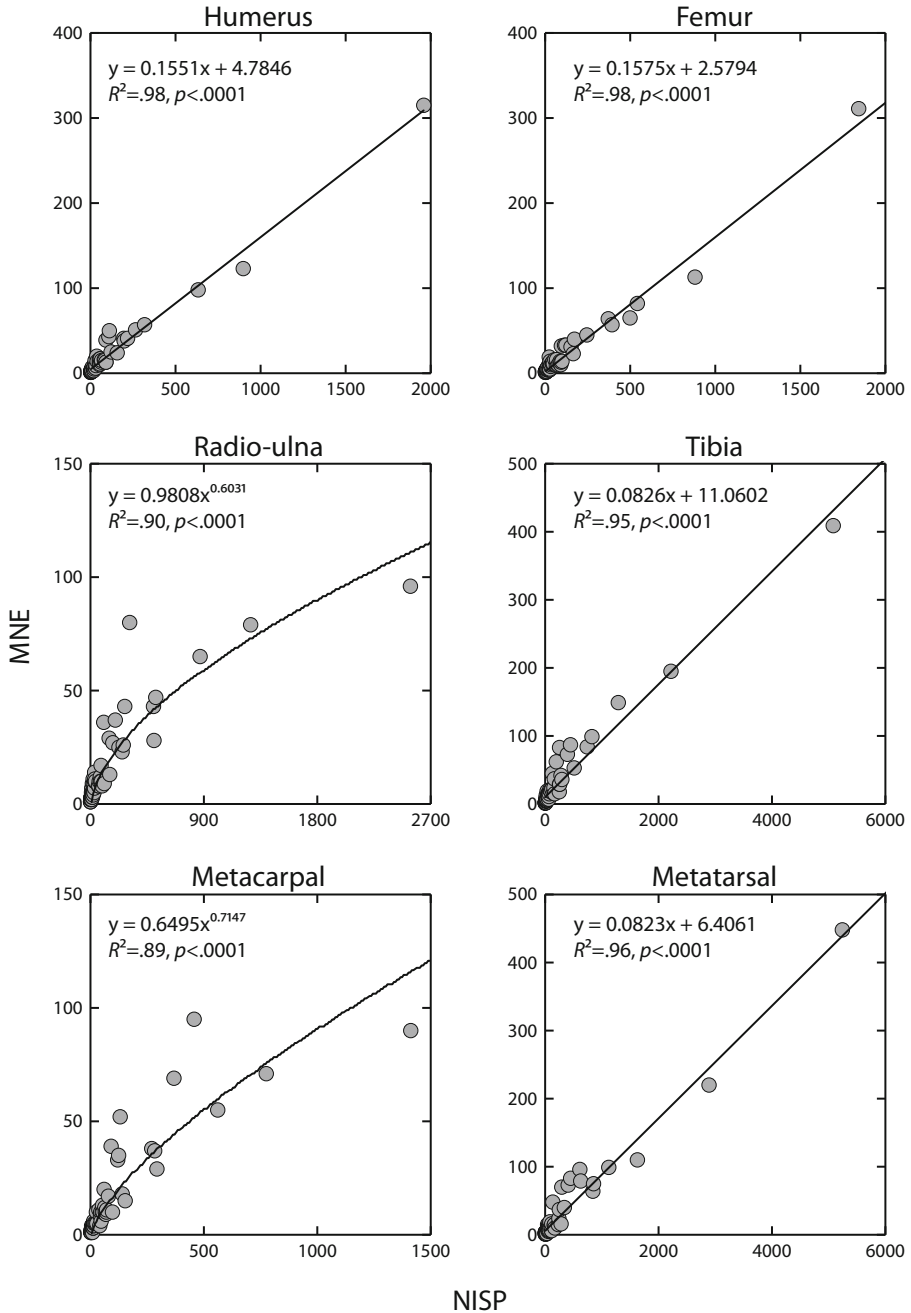


Fig. 1 NISP-MNE relationships for classes of long bones in a sample of Paleolithic assemblages. Only the best-fit line is shown for each class of elements (see Table 2)

Excluding large collections (NISP >50) from the correlations provides information on the numerical response of MNE to changes in NISP in small

assemblages. In the small samples (Table 3, Figs. 2, 3, 4, and 5), the relationships between the two metrics are generally better described by a power ($n = 17$) rather than a linear function ($n = 5$), the difference in frequencies between the two types of function being significantly different from chance ($\chi^2 = 6.5, p < 0.02$). The high number of elements for which a power function provides the best-fit model appears to confirm that MNE is, as predicted, curvilinearly related to NISP in small samples. The metatarsal is the only large bone that shows a stronger fit with a linear function. However, this probably reflects sampling error, as the power function gives the best fit model for this bone at a smaller threshold value for sample size, although the relationship is not significant (linear: $R^2 = 0.03, p = 0.50$; power: $R^2 = 0.11, p < 0.15, NISP \leq 30$). The other elements that yield a better fit with a linear function—the atlas, axis, hyoid, and small tarsals—all show very minor differences between NISP and MNE estimates.

Table 3 Best-fit relationships between NISP and MNE data for a sample of Paleolithic assemblages with NISP size ≤ 50

	Linear Function		Power Function	
	R^2	equation	R^2	equation
long bones				
humerus (n=32)	0.70	$y = 0.3308x + 0.8569$	0.74	$y = 0.9391x^{0.6615}$
radio-ulna (n=32)	0.67	$y = 0.2479x + 1.3451$	0.79	$y = 1.0074x^{0.6015}$
metacarpal (n=30)	0.62	$y = 0.1528x + 1.6776$	0.71	$y = 0.8532x^{0.5784}$
femur (n=34)	0.63	$y = 0.2514x + 1.521$	0.75	$y = 0.9407x^{0.6417}$
tibia (n=26)	0.55	$y = 0.2567x + 1.4195$	0.71	$y = 0.9695x^{0.6209}$
metatarsal (n=22)	0.51	$y = 0.1827x + 1.2775$	0.33, $p < .01$	$y = 1.1124x^{0.4402}$
large non-lbn				
cranium (n=25)	0.24, $p < .02$	$y = 0.0824x + 1.5765$	0.43, $p < .001$	$y = 1.0333x^{0.364}$
mandible (n=22)	0.44, $p < .001$	$y = 0.1386x + 2.0687$	0.54	$y = 1.3993x^{0.4039}$
scapula (n=39)	0.73	$y = 0.1909x + 1.3478$	0.83	$y = 0.9289x^{0.59}$
rib (n=20)	0.32, $p < .01$	$y = 0.2186x + 1.7107$	0.51, $p < .001$	$y = 0.8007x^{0.6263}$
innominates (n=38)	0.75	$y = 0.2187x + 1.6601$	0.84	$y = 1.0307x^{0.6107}$
vertebrae				
atlas (n=14)	0.89	$y = 0.7599x + 0.1633$	0.88	$y = 0.9436x^{0.8642}$
axis (n=11)	0.94	$y = 0.7405x + 0.4016$	0.86	$y = 0.9574x^{0.9}$
other cerv. (n=16)	0.78	$y = 0.45x + 0.2596$	0.88	$y = 1.0345x^{0.658}$
thoracic (n=19)	0.46, $p < .001$	$y = 0.3875x + 0.9104$	0.68	$y = 0.9152x^{0.6702}$
lumbar (n=20)	0.83	$y = 0.1914x + 1.318$	0.84	$y = 0.9256x^{0.5953}$
sacrum (n=11)	0.88	$y = 0.6282x + 0.4349$	0.94	$y = 1.0007x^{0.8038}$
small/short bones				
hyoid (n=9)	0.83, $p = .0001$	$y = 0.326x + 0.8745$	0.76, $p < .01$	$y = 1.0118x^{0.6086}$
carpals (n=37)	0.73	$y = 0.749x + 0.8017$	0.84	$y = 1.0426x^{0.876}$
malleolus (n=18)	1.00	$y = 0.9708x + 0.1471$	1.00	$y = 1.0026x^{0.9963}$
talus (n=28)	0.97	$y = 0.844x + 0.122$	0.99	$y = 1.0247x^{0.926}$
calcaneus (n=31)	0.95	$y = 0.5956x + 0.9277$	0.96	$y = 0.9927x^{0.8656}$
other tarsals (n=27)	0.95	$y = 0.8554x + 0.1566$	0.93	$y = 0.9909x^{0.931}$
phalanges (n=32)	0.95	$y = 0.7825x + 0.0409$	0.95	$y = 0.9223x^{0.9391}$

The number of assemblages that could be included in the regression analysis is given in parentheses in the leftmost column. A gray background identifies the relationship with the highest coefficient of determination (R^2) for a given skeletal element. All results are significant at <0.0001 except when specified otherwise. Within a class of elements, NISP counts were combined for all bone regions, whereas the MNE value was derived from the best represented bone portion. In case of conflicting counts, the highest NISP or MNE value reported was used in the calculations. The raw data can be consulted in the SOM, Table 1

The above-mentioned findings mean that MNE tends to inflate the representation of poorly represented elements, similar to the way in which MNI exaggerates the representation of individuals in small assemblages (Ducos 1968; Casteel 1977; Grayson 1978a, b, 1984; Lyman 2008; Cannon 2013). This finding implies that the calculation of MNE values is influenced by the size of the NISP sample. The trend for MNE values to increase at a decelerating rate relative to NISP likely follows from the decreasing probability of identifying new elements as NISP increases (Lyman 2008).

What our results also indicate is that MNE tallies may not increase proportionally *between* classes of skeletal parts, a problem illustrated in Fig. 6. Indeed, some classes of elements, such as the cranium, mandible, hyoid, scapula, vertebrae other than the atlas and axis, ribs, innominates, and the long bones, have a low scaling exponent, which is indicative of a strongly curvilinear relationship. Conversely, the atlas, axis, carpals, tarsals, malleolus, and phalanges show a high scaling exponent, which is indicative of a weakly curvilinear relationship. Because archaeological samples often differ widely in NISP size and skeletal composition, the fact that different elements do not always increase proportionately severely constrains the usefulness of MNE as a proxy measure of skeletal abundance.

While scaling exponents shed light on the numerical response of MNE to an increase in NISP size, comparisons of the coefficients of determination may provide information about variation in reproducibility of tallies between classes of parts. Indeed, holding the assemblages equal, elements that are easily and consistently counted should produce high NISP-MNE correlations, whereas a wide scatter of MNE values at comparable NISP sizes likely indicates that the abundance of the part of interest is more difficult to calculate. In the Paleolithic dataset, the small samples indicate a trend for the thoracic vertebrae, mandible, ribs, and more particularly, the cranium and metatarsal to show only moderate relationships ($R^2 = 0.33\text{--}0.68$, power function) between NISP and MNE data. The increased data dispersion observed in these elements may reflect a problem of reproducibility of the tallies (Fig. 7). Conversely, the relationships are very strong ($R^2 = 0.84\text{--}1.00$, power function) for the cervical and lumbar vertebrae, the sacrum, innominates and most of the small/short bones (*i.e.*, carpals, malleolus, tarsals, phalanges). These very strong relationships indicate that methods of calculation have only a small impact on the MNE values for these parts, presumably because they are mostly represented—as suggested by our own experience with some of these assemblages—by relatively complete specimens or by fragments with the same landmarks. If the above-mentioned assumptions are correct, these observations suggest that classes of parts are not always comparable in terms of MNE reproducibility.

In this dataset, reproducibility seems substantially lower than among the blind test participants (see Morin *et al.*, part I, this issue). This difference is easily explained. While Paleolithic specialists use a wide variety of methods for deriving MNE values, the subjects who participated in the blind test received very specific instructions about how to tally elements, which likely considerably increased reproducibility. This strategy was deliberate as the goal of the blind test was to produce a conservative test in which counting methods were as comparable as possible between the subjects.

Yet, in actual practice, archaeozoologists often diverge greatly in the way they generate MNE counts (Lyman 1994, 2008; Marean *et al.* 2001; Reitz and Wing

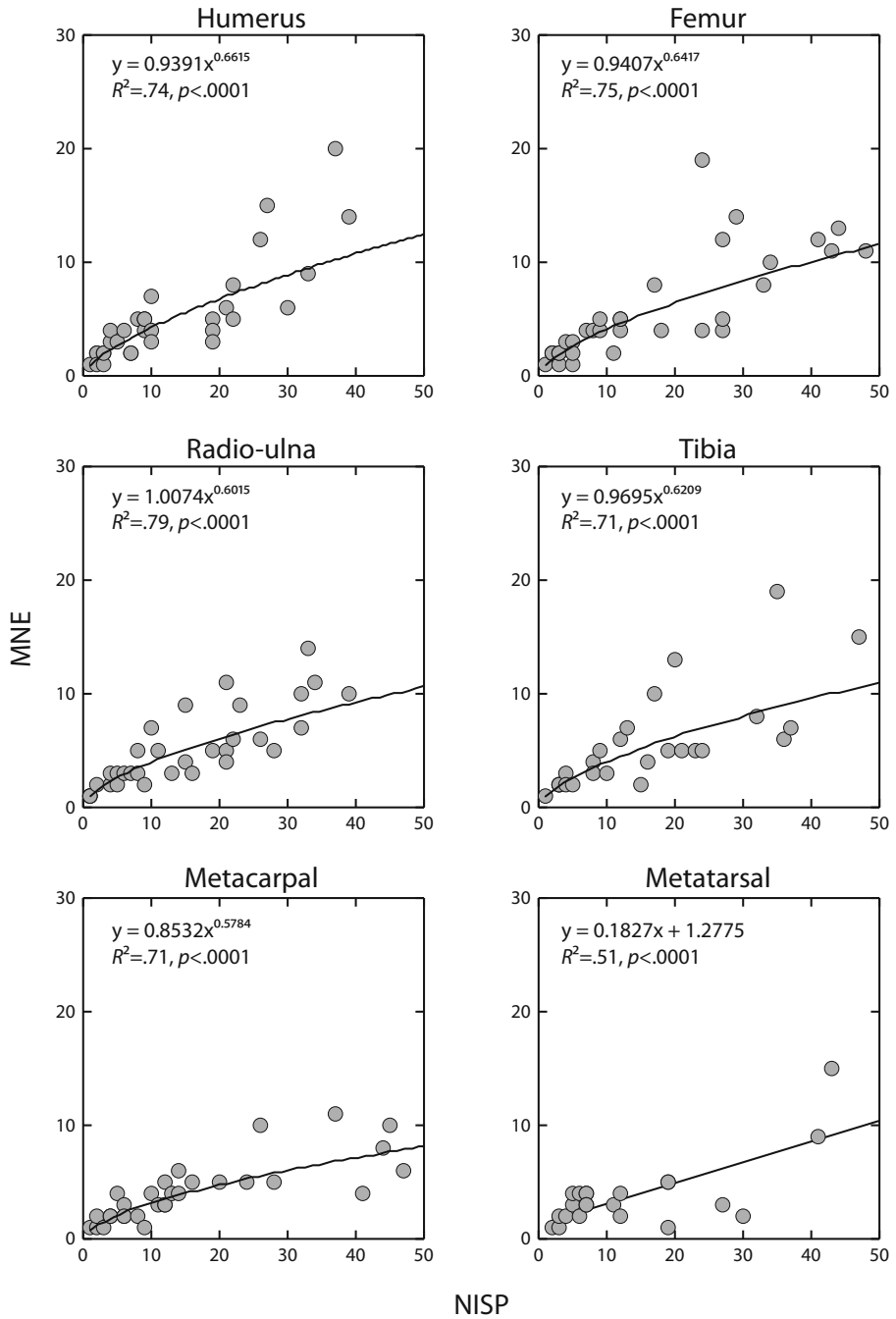


Fig. 2 NISP-MNE relationships for classes of long bones in a sample of Paleolithic assemblages with NISP sample size ≤ 50 . Only the best-fit line is shown for each class of elements (see Table 3)

2008). For instance, some analysts identify new elements by looking for overlap between fragments manually (e.g., Bunn and Kroll 1986) or using GIS software

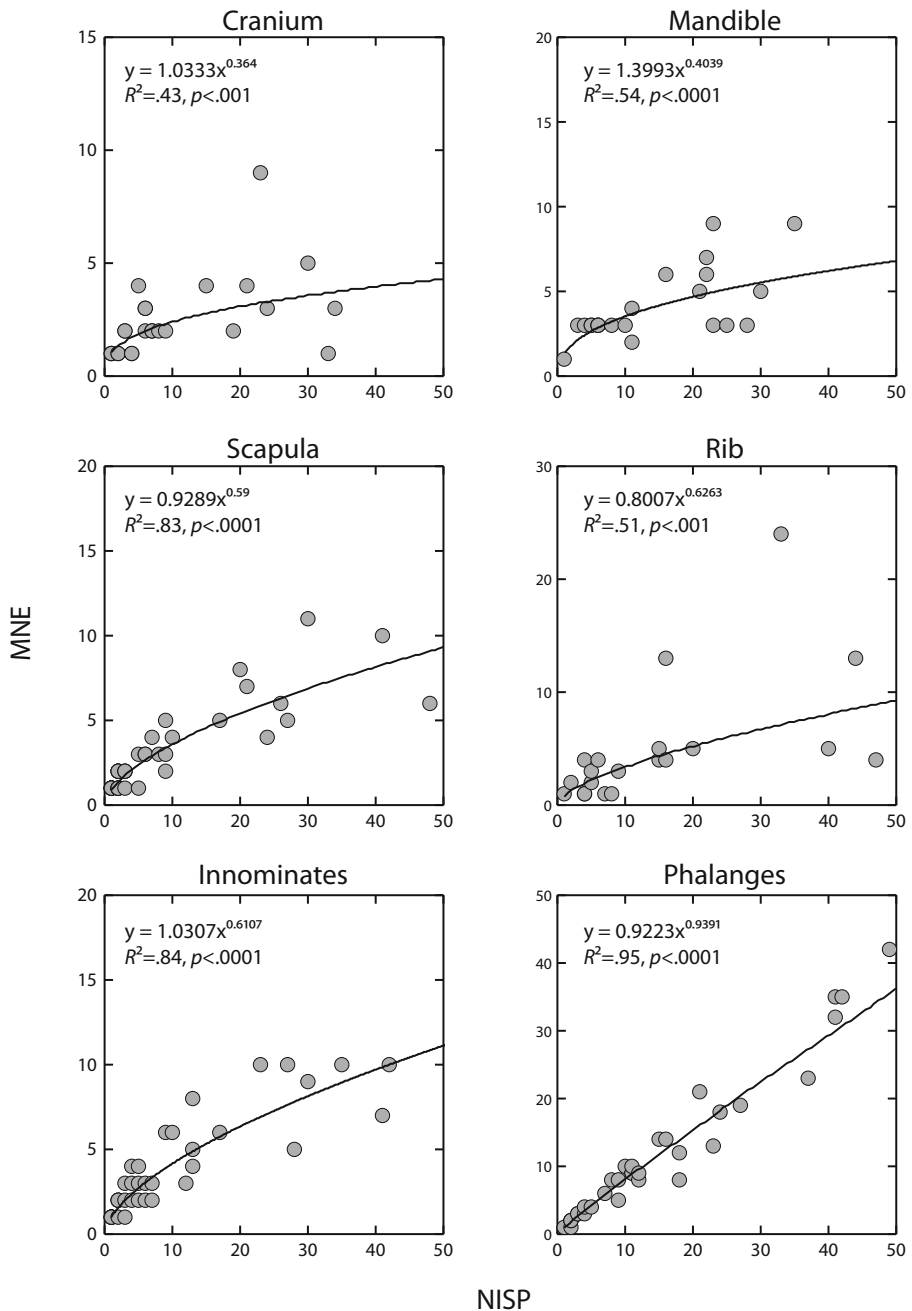


Fig. 3 NISP-MNE relationships for six classes of skeletal elements in a sample of Paleolithic assemblages with NISP sample size ≤ 50 . Only the best-fit line is shown for each class of elements (see Table 3)

(e.g., Marean *et al.* 2001), whereas others prefer to sum fractions in specific zones of bones (Klein and Cruz-Urbe 1984). Moreover, there is much variation between authors

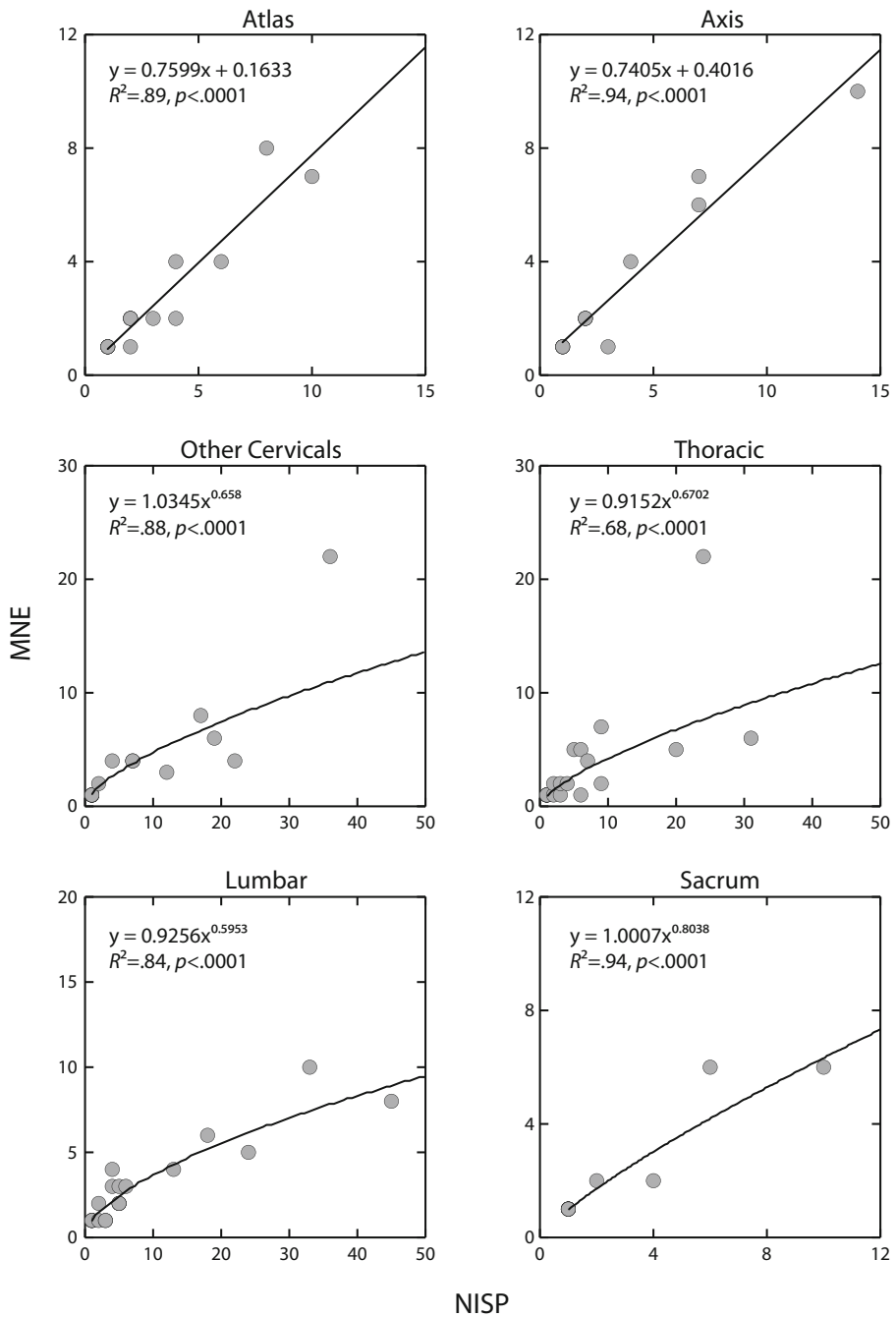


Fig. 4 NISP-MNE relationships for elements of the spine in a sample of Paleolithic assemblages with NISP sample size ≤ 50 . Only the best-fit line is shown for each class of elements (see Table 3)

in the consideration of criteria relating to sex, age, size, and morphological idiosyncrasies when identifying new elements. Studies have also highlighted major disparities in

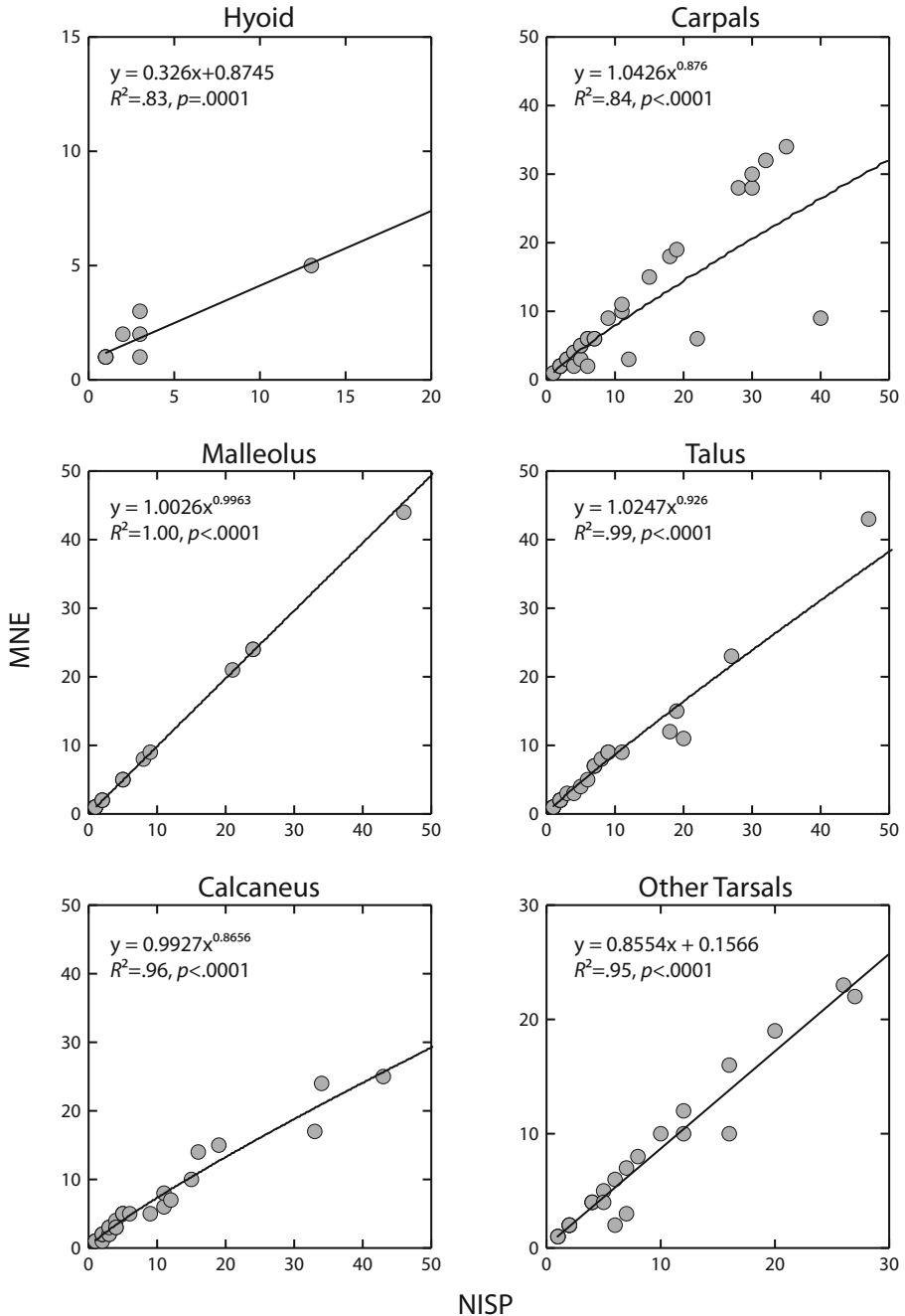


Fig. 5 NISP-MNE relationships for six classes of short/small elements in a sample of Paleolithic assemblages with NISP sample size ≤ 50 . Only the best-fit line is shown for each class of elements (see Table 3)

how faunal specialists treat long bone shaft fragments in their tallies: some consider them to be critical (Bunn 1991; Marean and Kim 1998; Pickering *et al.* 2003; Cleghorn

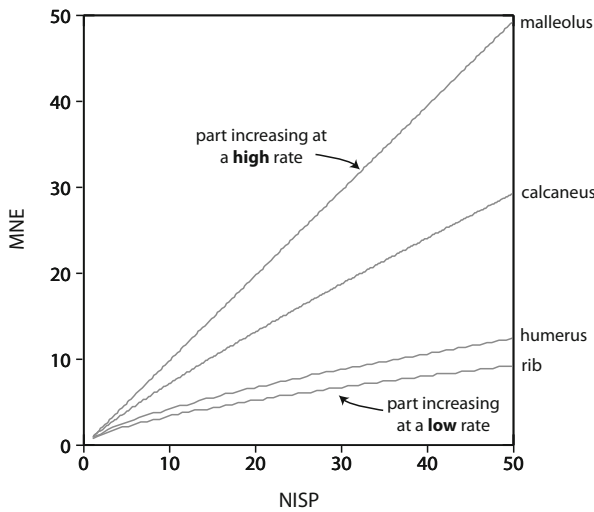


Fig. 6 Plot showing the shape of the NISP-MNE curve for four skeletal elements. The data are the same as those displayed in Figs. 2, 3 and 5. Note that the scales are harmonized in the present figure

and Marean 2004), while others believe they can be safely ignored (Klein *et al.* 1999; Stiner 2002). Thus, results obtained with MNE in real archaeological applications are much more variable than suggested by the blind test. However, our experiments indicate that the problem does not necessarily lie in the measure itself, but in a lack of consensus about how MNE values should be calculated in archaeological contexts.

Other problems have been identified with MNE. Estimates based on the minimum number concept suffer from the notorious problem of aggregation

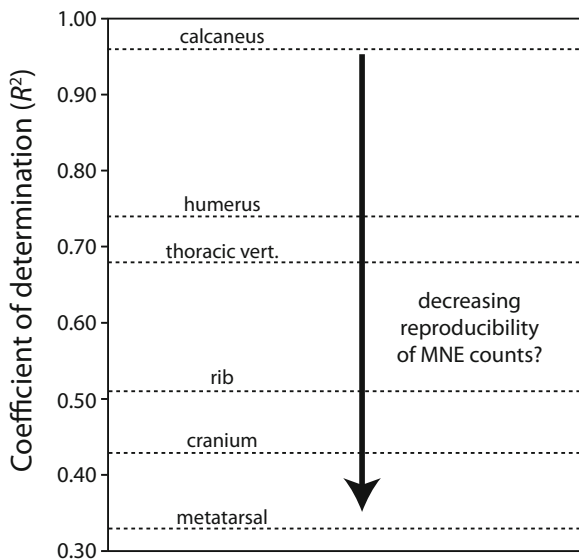


Fig. 7 Plot showing the coefficients of determination (R^2) for six skeletal elements. The R^2 values are those given in Table 3. Note that, in the sample of Paleolithic assemblages, the metatarsal is mostly represented by shaft fragments, which probably explains the low coefficients of determination obtained for this bone

(Paaver 1958 [cited in Casteel 1977]; Grayson 1973, 1979, 1984; Lyman 1994, 2008). Indeed, the fact that MNE values need to be recalculated after a new field season or when stratigraphic and/or spatial units are modified at a site is a major drawback as it slows the process of analysis and publication. Moreover, Grayson (1973, 1979, 1984) showed that different aggregation approaches applied to the same assemblage can alter the rank order of taxa at a site when tallies are based on the minimum number concept. As emphasized by Grayson (1984) and Lyman (2008), the problem of aggregation significantly undermines the value of MNE as a tallying method. This and the other issues raised earlier confirm that MNE is an imperfect measure of skeletal abundance. A different approach discussed below circumvents many of the pitfalls associated with this method.

An Alternative Metric: the Number of Distinct Elements

The many, sometimes daunting, problems associated with NISP, MNE, and MNI have led several specialists to explore alternative metrics of skeletal and taxonomic abundance (e.g., Davis 1992; Albarella and Davis 1996; Broughton 2004). Here, we discuss a different type of estimate that focuses on the abundance of specific landmarks. This metric, referred to as the Number of Distinct Elements (NDE), simply tallies the number of times a diagnostic landmark is represented in a sample of specimens attributed to the same element and taxon. In this approach, a landmark gives a NDE tally of “1” *if and only if the fragment shows at least 50 % of the cortical surface of that landmark*. This is a safeguard to avoid counting the same element more than once. Although developed independently, this approach is similar in design to one devised by Watson (1979) for ungulates, and to counting systems implemented by archaeomalacologists (Mason *et al.* 1998; Harris *et al.* 2015).

With respect to vertebrates, the main differences between the NDE and Watson’s “diagnostic zone” approach lie in how landmarks are defined. The landmarks used in the NDE tend to cover smaller regions of bones, include a wider range of elements and bone regions (such as shaft fragments, sesamoids, ribs, and vertebrae), and are assessed using a control cutout. Moreover, in contrast to Watson’s method, left and right sides of paired elements are not treated as separate landmarks in the NDE, although these can be distinguished in a database. Despite these differences, both approaches share the same goal of tallying distinct elements with the aid of a pre-determined list of landmarks.

An example will illustrate how NDE estimates are generated. In a sample of five red deer mandible specimens, three left and one right fragments give an NDE of 4 for the mandibular condyle because this landmark is mostly or fully represented on all four remains (Fig. 8). This tally excludes the fifth fragment that only comprises a small fraction of the landmark (the rightmost specimen in Fig. 8). This specimen is ignored in the NDE approach because future samples from the same archaeological context may comprise the associated fragment that contains most of the landmark. Indeed, as pointed out by Watson (1979, pp. 129–130), because the aim is to avoid counting the same element twice, one must: “reject any piece that does not have more than half the zone present.” Importantly, to reduce subjectivity and increase standardization, a small square cutout (shown as black squares in Fig. 8) provides a control for assessing

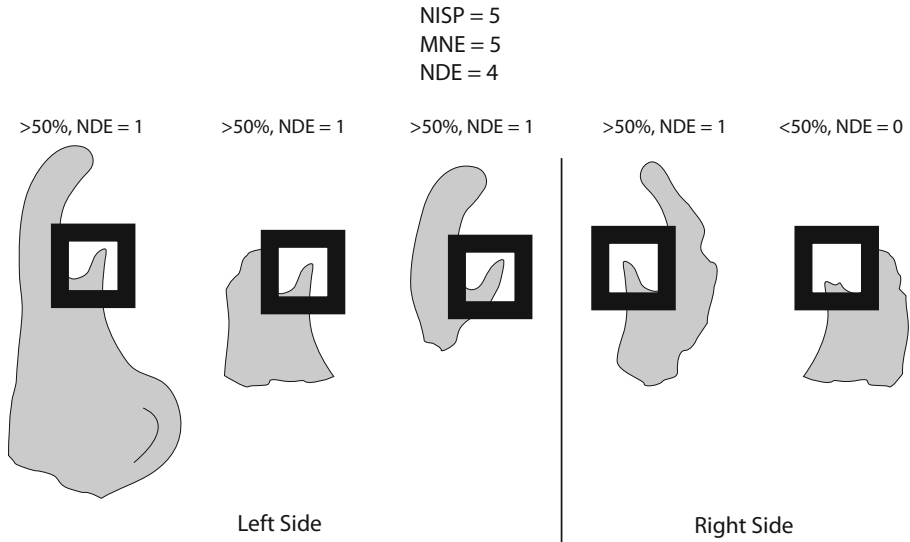


Fig. 8 Calculation of NDE values in a sample comprising five red deer mandible specimens. Because the rightmost specimen shows less than 50 % of the cortical surface of the landmark, it was not included in the total NDE. The control cutout shown here has an internal side of 15 mm

whether at least 50 % of the cortical surface of the landmark is preserved. Concerning foramina, the NDE count only includes specimens that comprise at least half of the external circumference of the foramen.

We note that the size of the cutout may need to be adapted to the size of the species. For small- (<50 kg), moderate- (50–250 kg) and large-sized (>250 kg) species, we suggest using control cutouts with an internal side of 10, 15, and 25 mm, respectively. We also note that for purposes of standardization, the cutout is invariably of the same shape (a square) and dimensions for a given body size class and is preferably made of flexible material (*e.g.*, fabric, plastic wrapping) so that it can be placed on the surface of bones with different morphology. In all cases, the landmark must lay at the center of the cutout.

For cervids and bovids, the NDE is based on 87 landmarks covering all classes of skeletal elements (Table 4). This list includes many “point-specific” landmarks that are likely to occur even on small fragments, such as nutrient foramina, fossae, eminences, the base of processes, and small articular surfaces. To ensure consistent coverage of all portions of the long bones, four landmarks were selected for each class of long bones: one for each epiphysis and one for each of the shaft halves (Fig. 9). For cervids, we include a fifth landmark—length of the anterior groove in millimeters (Castel 1999)—for the metatarsal and metacarpal because there are no point-specific landmarks on the shaft of these bones, but only long homogeneous diagnostic zones (Fig. 10). To derive an NDE value for the metatarsal and metacarpal, the summed measurements obtained for this landmark are divided by the known length of a metatarsal or metacarpal similar in dimensions to those reconstructed for the assemblage. For skeletal elements other than long bones (Fig. 11), between one and three landmarks were selected, generally as a function of the size of the bone.

Landmarks were generally chosen on the basis of their susceptibility of being identified in highly fragmented assemblages, as well as experience with archaeological material. It is important to note that, when calculating the total for a class of elements with multiple landmarks, only *the NDE value from the most common landmark* is retained. This is crucial as it ensures that the tallies are truly independent at the level of the element. To illustrate this point, two examples are given in Fig. 12. In this figure, the NDE for the tibia is “6,” and that for the mandible is “5.” Having multiple landmarks is also useful because they allow for intra-element comparisons of patterns of representation.

In addition to the study of skeletal abundances, the NDE can be used as a proxy measure of taxonomic representation. However, NDE tallies will normally need to be adjusted because species tend to differ in frequencies of bones. In a manner reminiscent of the MAU routine (Binford 1984), normed NDE (NNDE for short) values are derived by dividing the NDE count for an element by the abundance of the same element in a living animal. The NNDE values can then be summed (Σ NNDE) to obtain a total standardized element count for each taxon. The NDE is thus a flexible measure as it can be used to estimate both skeletal and taxonomic abundances.

Comparisons of the NDE and MNE Approaches

Because it was developed late in the course of this research, the NDE approach could not be integrated in the blind test discussed in part I. Nonetheless, NDE values were derived by the first author (see Appendix Table 7) for the experimental samples presented in part I and compared with the actual numbers of elements (ANE). Unfortunately, the author’s prior knowledge about the composition of the samples and other factors (long bone specimens in one experiment were extensively refitted for another experiment) restrain the power of this “test,” although efforts were made to ignore these favorable conditions during the counting procedure. The results presented below therefore provide only a preliminary assessment of the accuracy of the NDE.

Before discussing the results of this test, some information must be presented about the experimental samples that were used as a control. The two samples comprise a large number of red deer (*Cervus elaphus*, Σ ANE = 501, samples combined) and a few cattle (*Bos taurus*, Σ ANE = 5, samples combined) elements, mostly long bones from the former species. In the first experiment (called the marrow-cracking experiment (MCE)), elements were only marrow-cracked, whereas in the second experiment (called the bone grease rendering experiment (BGRE)), elements were marrow-cracked and subsequently processed for bone grease. Detailed records were kept of initial abundances and specimen counts. Additional information about the samples can be found in part I.

Rank order correlations between the NDE and ANE values are very strong in the MCE and BGRE for all elements, and for the sample that excludes long bones (Table 5). As was the case with MNE (see part I), the relationship for long bones is weaker in the MCE. The data also indicate that the performance of the two metrics is similar for long bone regions (Table 6). Comparisons at the taxonomic level show no statistical difference between the Σ NDE and

Table 4 Landmarks that form the basis of the NDE for cervids and bovids

Ldmk#	Landmarks
Humerus	
1	Lmk1 (base of the greater tubercle)
2	Lmk2 (base of the <i>Tuberositas teres major</i>)
3	Lmk3 (foramen)
4	Lmk4 (fossa of the <i>Capitulum</i>)
Radius	
5	Lmk1 (<i>Tuberositas radii</i>)
6	Lmk2 (proximal surface of the articular surface with the ulna)
7	Lmk3 (medial anterior ridge of the distal radius)
8	Lmk4 (radial styloid process)
Ulna	
9	Lmk1 (constriction of the olecranon)
10	Lmk2 (proximo-medial portion of the trochlear notch)
11	Lmk3 (lateral coronoid process)
12	Lmk4 (ulnar styloid process)
Metacarpal	
13	Lmk1 (anterior portion of the ridge separating the two main proximal articular surfaces)
14	Lmk2 (proximal portion of the anterior groove)
15	Lmk3 (anterior portion of the distal metacarpal canal)
16	Lmk4 (fossa of the medial condyle + fossa of the lateral condyle)/2
17	Lmk5 (length measurement of the anterior groove ^a)
Femur	
18	Lmk1 (<i>Fovea capitis</i>)
19	Lmk2 (foramen)
20	Lmk3 (proximal portion of the <i>Fossa supracondylaris</i>)
21	Lmk4 (posterior portion of the facet on the axial face of the lateral condyle)
Tibia	
22	Lmk1 (<i>Sulcus extensorius</i>)
23	Lmk2 (distal portion of the foramen)
24	Lmk3 (constriction of the posterior ridge)
25	Lmk4 (medial malleolus)
Metatarsal	
26	Lmk1 (anterior portion of the ridge separating the two main proximal articular surfaces)
27	Lmk2 (proximal portion of the anterior groove)
28	Lmk3 (distal portion of the anterior groove)
29	Lmk4 (fossa of the medial condyle + fossa of the lateral condyle)/2
30	Lmk5 (length measurement of the anterior groove ^a)

Table 4 (continued)

Ldmk#	Landmarks
	Indeterminate metapodial
31	(fossa of the medial condyle + fossa of the lateral condyle)/2
	Other bones
32	Antler (base, >50 % of the circumference); for bovids: tip of horncore
33	Cranium (worn or unworn UD4 + worn UM3)/2; mesial lobe ^b
34	(petrosal, >50 %)/2
35	Mandible (worn or unworn LD4 + worn LM3); mesial lobe ^b
36	(<i>Foramen mentale</i>)
37	(mandibular condyle)
38	Hyoid (proximal section of the stylohyoideum, >50 %)
39	(epihyoideum, >50 %)
40	(basihyoideum, proximal section, >50 %)
41	Atlas (cranial view, left articular surface)
42	(caudal view, inter-articular notch)
43	Axis (middle portion of the <i>Dens axis</i>)
44	(dorsal section of the cranial articular surface, left side)
45	Other cervical vertebrae (base of the spinous process, anterior side)
46	(cranial articular process, left side)
47	Thoracic vertebrae (cranial articular surface, left side)
48	(cranial <i>Fovea costalis</i> , left side)
49	Lumbar vertebrae (cranial articular surface, left side)
50	(medio-anterior portion of the transverse process)
51	Sacrum (left portion of the cranial surface of the centrum)
52	(dorsal extremity of the spinous process of the 2nd sacral vertebrae)
53	Caudal vertebrae (centrum, cranial side)
54	Rib (proximal end)
55	(distal end)
56	Sternebrae (>50 % of the bone)
57	Scapula (dorsal portion of the glenoid cavity)
58	(base of the acromion)
59	(constricted portion of the distal axillary border)
	Carpals
60	Scaphoid (>50 %)
61	Lunatum (>50 %)
62	Triquetrum (>50 %)
63	Pisiform (>50 %)
64	Capitatum (>50 %)
65	Hamatum (>50 %)
66	Innominate (foramen on the dorsal side of the ilium)
67	(acetabulum: ischium portion)
68	(acetabulum: pubis portion)

Table 4 (continued)

Ldmk#	Landmarks
69	Patella (anterior view, central portion)
70	(posterior view, apex)
71	Malleolus (distal view, articular surface)
	Tarsals
72	Talus (proximal portion of the lateral surface)
73	(proximal portion of the medial surface)
74	Calcaneus (posterior portion of the <i>Tuber calcanei</i>)
75	(anterior portion of the articular surface for the talus)
76	(distal extremity, articular surface for the cubo-navicular)
77	Cubo-navicular (anterior portion of the articular surface for the calcaneus)
78	Smaller cuneiform (>50 %)
79	Greater cuneiform (>50 %)
80	Phalanx 1 (portion of the proximal articular surface near the anterior aspect)
81	Phalanx 2 (portion of the proximal articular surface near the anterior aspect)
82	Phalanx 3 (portion of the proximal articular surface near the anterior aspect)
83	Vestigial phalanx 1 (>50 %)
84	Vestigial phalanx 2 (>50 %)
85	Vestigial phalanx 3 (>50 %)
86	Vestigial metapodial (>50 %)
87	Sesamoids (>50 %)

^a See text and Fig. 10 for an explanation of the measurement method

^b Only teeth showing more than 50 % of the occlusal surface for the mesial lobe are counted

Σ ANE (MCE: $\chi^2 = 0.2$, $p = 0.68$; BGR: $\chi^2 = 0.1$, $p = 0.72$, whole bone counts, vestigial metacarpals excluded [see Table 5, note 1], Σ NDE counts from Appendix Table 7, raw NDE values were used because the two species comprise the same skeletal frequencies for the elements considered). These observations suggest that the NDE is as robust as MNE for estimating skeletal, and possibly, taxonomic abundances.

Advantages and Limitations of the NDE Approach

In addition to yielding promising experimental results, NDE has five advantages over MNE. These include the following:

1. NDE counts are more easily calculated than MNE counts.
2. The measure is inherently more standardized than the MNE method.
3. NDE values are expected to increase linearly with NISP sample size.

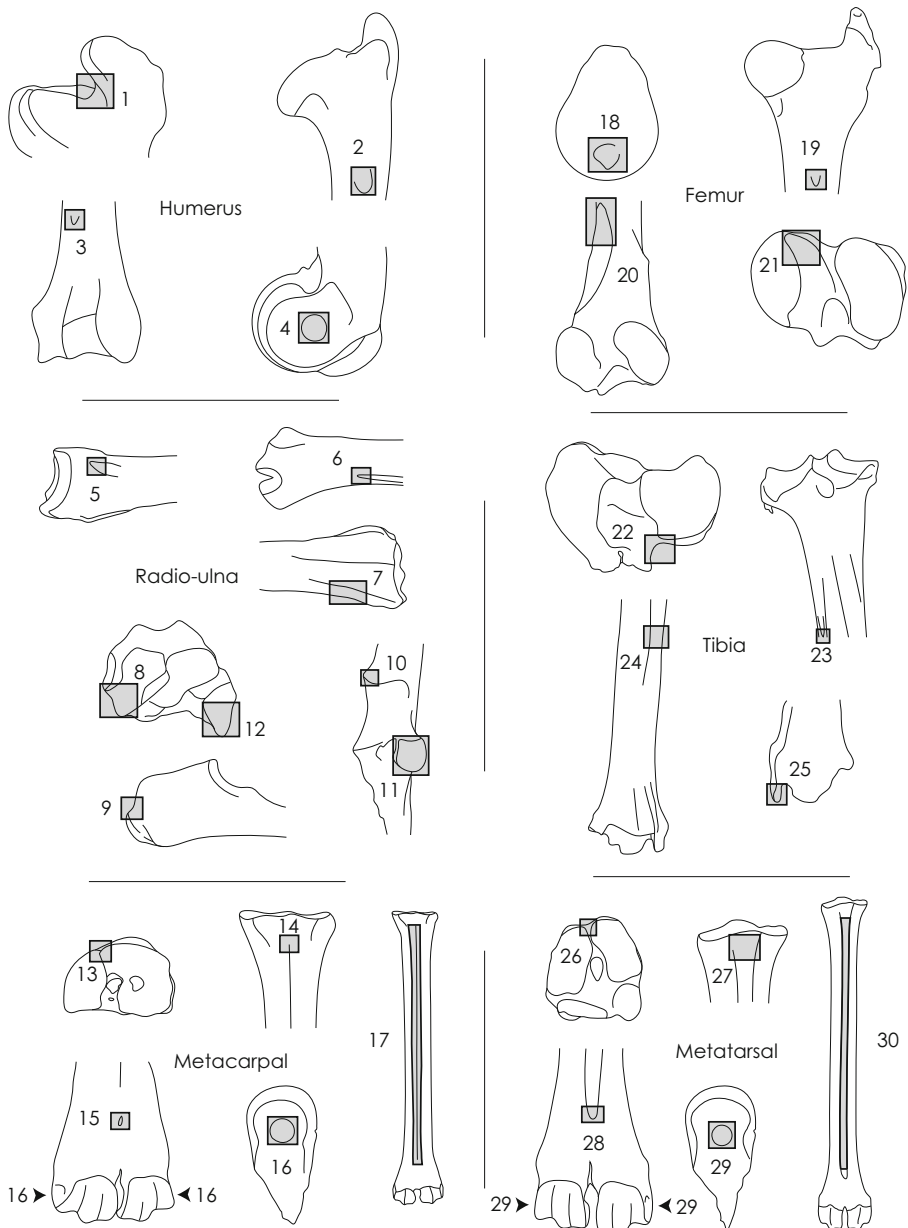


Fig. 9 Location of landmarks for cervid and bovid long bones. The landmarks are described in Table 4. All images of elements are from the left side. The bones were drawn by François Lacrampe-Cuyaubère, Archéosphère

4. The NDE approach does not suffer from the problem of aggregation.
5. NDE counts facilitate comparisons with recent approaches to calculating mollusk abundance.

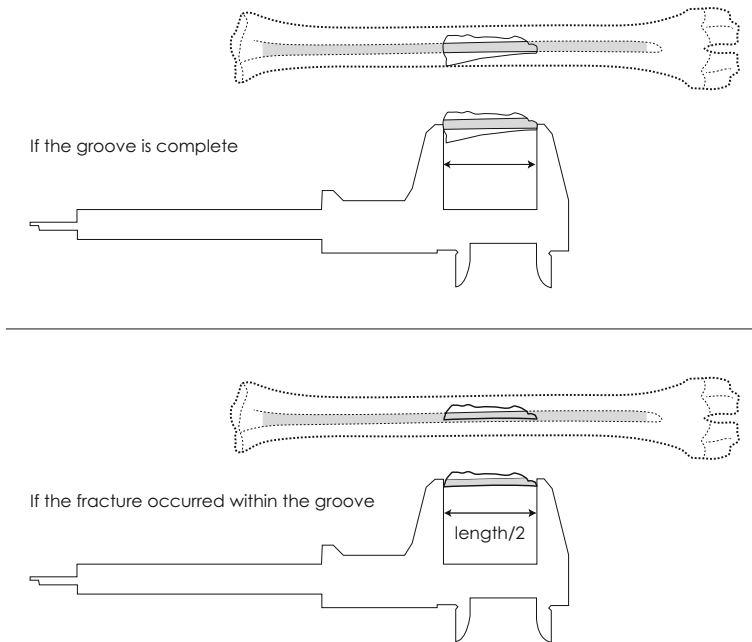


Fig. 10 Method used to calculate measurement length in mm for the metatarsal and metacarpal. See text for explanation

The first point is relatively straightforward. The NDE approach eliminates the time-consuming task of spreading/drawing the material and looking for overlaps between specimens (see Marean *et al.* [2001] for a review of overlap methods with MNE). With the NDE, the tallying process simply involves identifying a diagnostic landmark and tabulating it. Thus, NDE totals can be generated at any point during analysis, for instance, by counting the number of times a given landmark is recorded as present in a spreadsheet column. In the example provided in Fig. 13, tallies are easily calculated: the NDE for landmark #18 (femur, *Fovea capitis*) is “3,” that for landmark #22 (femur, *Sulcus extensorius*) is “2,” and that for landmark #23 (femur, foramen) is “1.” If needed, the side of a paired element can be identified by adding an “L” (for left) or an “R” (for right) next to the landmark number in the database. Moreover, because specimens counted by a single NDE landmark are, by definition, from distinct elements (each represents >50 % of the landmark), the problem of interdependence seen in NISP is also avoided.

The second advantage of NDE follows from the first. As discussed earlier, methods of MNE calculation are notoriously variable. Common sources of disagreement include whether specimens should be tallied as fractions or integers and whether long bone shaft fragments and criteria of sex, age, and size should be considered during the counting process (Klein and Cruz-Uribe 1984; Bunn 1991; Lyman 1994, 2008; Marean *et al.* 2001; Reitz and Wing 2008). In comparison, the NDE approach allows for greater standardization because the method focuses on a set of precise and invariable landmarks that are counted as integers. Moreover, criteria of sex, age, and size are not pertinent to the calculation of NDE values, and therefore, are ignored. The use of a

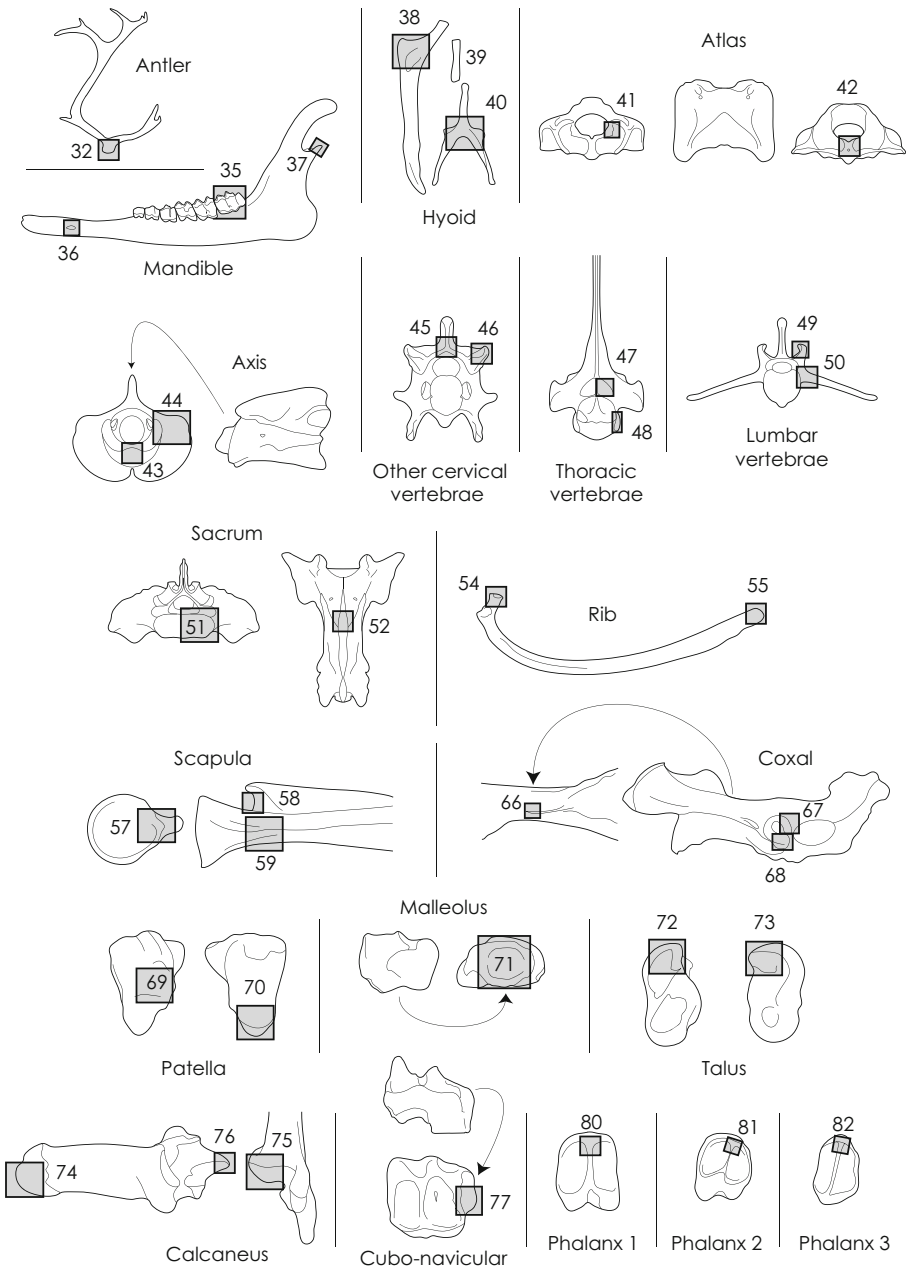


Fig. 11 Location of landmarks for cervid and bovid elements other than long bones. The landmarks are described in Table 4. Images of all paired elements are from the left side. The bones were drawn by François Lacrampe-Cuyaubère, Archéosphère

control cutout also contributes to reducing subjectivity. For these reasons, the approach should produce tallies that are more comparable between specialists and samples than those based on MNE.

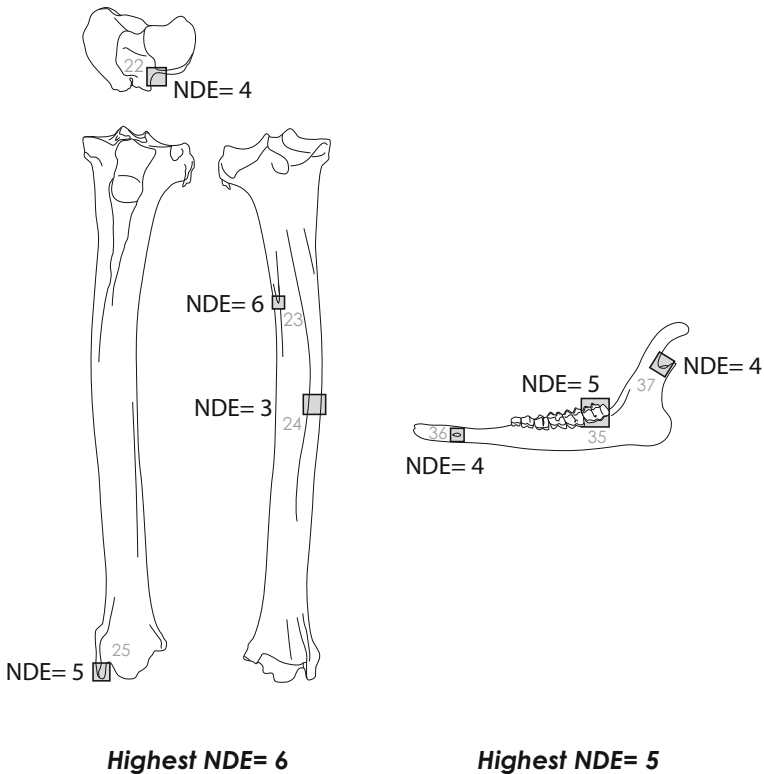


Fig. 12 Example of calculation of NDE estimates for the tibia and mandible

The third advantage with NDE is that it does not inflate the representation of rare elements. NDE values are expected to increase linearly with NISP because the probability of identifying a new element is *independent of previous identifications*. This is unlike MNE, as identifications of new elements are linked in this approach, which results in tallies increasing at a decelerating rate relative to NISP (Lyman 2008). However, analyses of large samples of paired NISP-NDE data will be required to verify these inferences.

A fourth advantage revolves around the issue of aggregation. Grayson (1973, 1979, 1984) pointed out that MNE (and MNI) values are not additive because skeletal elements are unlikely to be identically distributed across all excavation units. Indeed, due to the vagaries of sampling, the most common element in an excavation unit is likely to differ from the most common element in another or larger excavation unit (Ducos 1968; Grayson 1984). Figure 14 illustrates this difficulty by showing the same set of metatarsal specimens in two hypothetical situations: a floor plan consisting of two houses and a stratigraphy composed of two layers. In the house example, the total of the MNE values ($4 + 2 = 6$) is identical to the actual MNE value (“6”) for the aggregated houses because all the tallies were derived from the same landmark (identified by a polygon). In contrast, in the stratigraphic example, the MNE for layer A was derived from the landmark marked by a circle, whereas that for layer B was derived from a different landmark identified by a square. To complicate things even further, the MNE for the sample that combines the two layers was derived from a third landmark (marked

Table 5 Spearman's rank correlation tests of accuracy for MNE versus NDE

	All elements ($n = 18$) ^a		Long bones only ($n = 6$)		Other elements ($n = 12$)	
MCE						
MNE vs ANE						
Subject A	<i>0.97</i>	<i><0.0001</i>	0.80	=0.08	<i>0.93</i>	<i><0.01</i>
Subject B	<i>0.94</i>	<i><0.0001</i>	0.71	=0.11	<i>0.85</i>	<i><0.01</i>
Subject D	<i>0.93</i>	<i><0.0001</i>	0.44	=0.32	<i>0.84</i>	<i><0.01</i>
NDE vs ANE						
Post blind test	<i>0.96</i>	<i><0.0001</i>	0.63	=0.16	<i>0.93</i>	<i><0.01</i>
BGRE						
MNE vs ANE						
Subject A	<i>0.98</i>	<i><0.0001</i>	<i>0.94</i>	<i><0.04</i>	<i>0.95</i>	<i><0.01</i>
Subject B	<i>0.89</i>	<i><0.01</i>	0.43	=0.34	0.75	=0.13
Subject D	<i>0.96</i>	<i><0.0001</i>	0.70	=0.12	<i>0.89</i>	<i><0.01</i>
NDE vs ANE						
Post blind test	<i>0.93</i>	=0.0001	<i>0.99</i>	<i><0.03</i>	<i>0.76</i>	<i><0.02</i>

Subjects A, B, and D are those who participated in the blind test (data from Table 15 in Morin et al., Part I, this issue). Statistically significant results are in italics. For each class of elements, the highest NDE value (data in Appendix 1) was used in the calculations

^a The category "all elements" comprises 18 classes of elements: cranium, mandible, hyoid, rib, scapula, the six long bones (the radio-ulna was treated as a unit), carpals, innomates, malleolus, talus, calcaneus, the other tarsals combined, all phalanges. Note that the vestigial metacarpal was excluded from this table because the first author was at an unfair advantage relative to the blind test participants, as the preparation of the experimental samples increased his familiarity with this bone. In line with this modification, the results for the blind test participants in this table may differ slightly from those shown in Table 15 in Morin et al., Part I, this issue

by a polygon). Because the most abundant landmark differs between these three units, it is not surprising to find that the actual value for the aggregated layers (MNE = 6) conflicts with the total ($4 + 4 = 8$) of the MNE values for layers A and B.

Unlike MNE or MNI, the landmarks that provide the estimates in the NDE approach are constant and do not vary with the composition of the sample. The use of constant landmarks means that aggregation has no effect on the calculation of NDE counts. Figure 15 demonstrates this point by using the same set of metatarsal specimens shown in Fig. 14. In both the floor plan and stratigraphic examples, the NDE approach gives identical values ("5") for the aggregated samples. This aspect of the NDE is critical, as it indicates that counts for a given landmark can, like NISP tallies, be added indefinitely as long as the criteria of identification remain unchanged and that data are *reported for all landmarks*. Counts may not be fully additive if only published for whole bones, as the most common landmark may differ between excavation units for elements with multiple landmarks. Systematic reporting of all landmark data simply and effectively eliminates this potential problem. In avoiding the problem of aggregation, the NDE approach represents a marked improvement relative to the MNE.

The fifth advantage of NDE relates to the study of contexts where counts for vertebrates need to be compared with those for molluscs, a group of animals with a

Table 6 Spearman's rank correlation tests of accuracy in estimates of skeletal abundances for bone regions comparing MNE with NDE

	Epiphyseal regions ^a (<i>n</i> = 14)		Shaft regions ^b (<i>n</i> = 13)	
MCE				
MNE vs ANE				
Subject A	<i>0.83</i>	<i><0.01</i>	0.34	=0.24
Subject B	<i>0.92</i>	= <i>0.001</i>	0.28	=0.34
Subject D	<i>0.80</i>	<i><0.01</i>	<i>0.60</i>	<i><0.04</i>
NDE vs ANE				
Post blind test	<i>0.93</i>	<i><0.001</i>	0.35	=0.23
BGRE				
MNE vs ANE				
Subject A	0.51	=0.07	0.07	=0.80
Subject B	0.41	=0.14	0.21	=0.46
Subject D	0.45	=0.11	0.07	=0.82
NDE vs ANE				
Post blind test	0.43	=0.13	0.22	=0.44

Subjects A, B, and D are those who participated in the blind test (data from Table 16 in Morin et al., Part I, this issue). Statistically significant results are in italics. NDE values are taken from Appendix Table 7

^a Proximal epiphysis NDE values are for NDE landmarks #1, 5, 9, 13, 18, 22, 26. Distal epiphysis NDE values are for NDE landmarks #4, 8, 12, 16, 21, 25, 29

^b Proximal shaft NDE values are for NDE landmarks #2, 6, 14, 19, 23, 27. Distal shaft NDE values are for NDE landmarks #3, 7, 15, 20, 24, 28. For the ulna shaft, the highest value for NDE landmarks #10–12 was used

simplified exoskeleton (Claassen 1998). Recently, archaeomalacologists have turned to new methods for estimating the abundance of molluscan taxa using pre-determined “non-repetitive elements” (NRE) that provide the basis for the calculation of MNI values (Giovas 2009; Harris *et al.* 2015; Thomas and Mannino 2016). Of particular importance in this respect is Harris *et al.*'s (2015) extensive study aimed at standardizing NRE methods of calculation for a wide range of diagnostic landmarks, including hinges and umbos in bivalves and apices in univalves. In their approach, NRE-based MNI differ conceptually from vertebrate MNI because the former counts circumvent the problem of aggregation by tallying mutually exclusive specimens using pre-determined landmarks. This fundamental characteristic entails that the NRE-based MNI in Harris *et al.* (2015) is conceptually similar to the NDE. For this reason, the two approaches should enable sounder comparisons of vertebrate and invertebrate tallies than previous counting methods.

The above-mentioned features and the simplicity of the method make NDE a valuable substitute to traditional metrics such as MNE and MNI. Familiarizing oneself with the NDE does not take more than two or three hours of practice for an experienced

Taxon	Bodypart	Landmark	NDE#
<i>Cervus elaphus</i>	femur	<i>Fovea capitis</i>	18L
<i>Cervus elaphus</i>	femur	<i>Fovea capitis</i>	18L
<i>Cervus elaphus</i>	femur	<i>Fovea capitis</i>	18R
<i>Cervus elaphus</i>	tibia	foramen	
<i>Cervus elaphus</i>	tibia	<i>Sulcus</i> , foramen	22L, 23L
<i>Cervus elaphus</i>	tibia	<i>Sulcus</i>	22L

Fig. 13 An example showing how the NDE can be calculated from a spreadsheet. Numbers in the “NDE” column correspond to the landmark identification numbers in Table 4. For each identified specimen, a landmark ID number is entered only when at least half of the landmark is present. In this figure, the total NDE for landmarks #18, #22 and #23 are: 3 (2 lefts and 1 right), 2 (2 lefts) and 1 (1 left), respectively. Note that one of the specimens shows *two* landmarks. For this reason, both are tabulated. Alternately, the information can be recorded on two separate lines with an additional column indicating the specimen ID, which may be more suitable for many databases

analyst. Although the number of landmarks that one must pay attention to is relatively large, most of them are probably well known to the archaeozoologist. Importantly, a test of the approach with Paleolithic material has shown that the NDE only marginally affects analysis time relative to just tallying NISP and is considerably more efficient than methods commonly used for tabulating MNE. One current disadvantage with the NDE approach is that the landmarks in Table 4 are only relevant for cervids and most bovids. We hope in the near future to publish lists of landmarks for a large number of taxonomic groups (*e.g.*, equids, suids, carnivores). Another limitation of the method is that it may not be suitable when estimates need to be generated for bone portions that do not include a NDE landmark.

Discussion

As discussed in part I, MNE seems to avoid many biases inherent in NISP. However, comparisons of NISP-MNE data within classes of skeletal parts show a clear trend for the relationships to be curvilinear. The degree of curvilinearity seems to be mostly explained by fragmentation. In general, the more fragmented an element, the greater the tendency for the relationship to be curvilinear. This observation probably explains why rodent elements—more frequently recovered complete than ungulate elements—tend toward linearity in NISP-MNI comparisons (Grayson 1984; Lyman 2003, 2008).

The curvilinear relationships observed in the Paleolithic sample mean that MNE, like MNI, tends to inflate the representation of rare elements. Therefore, derived

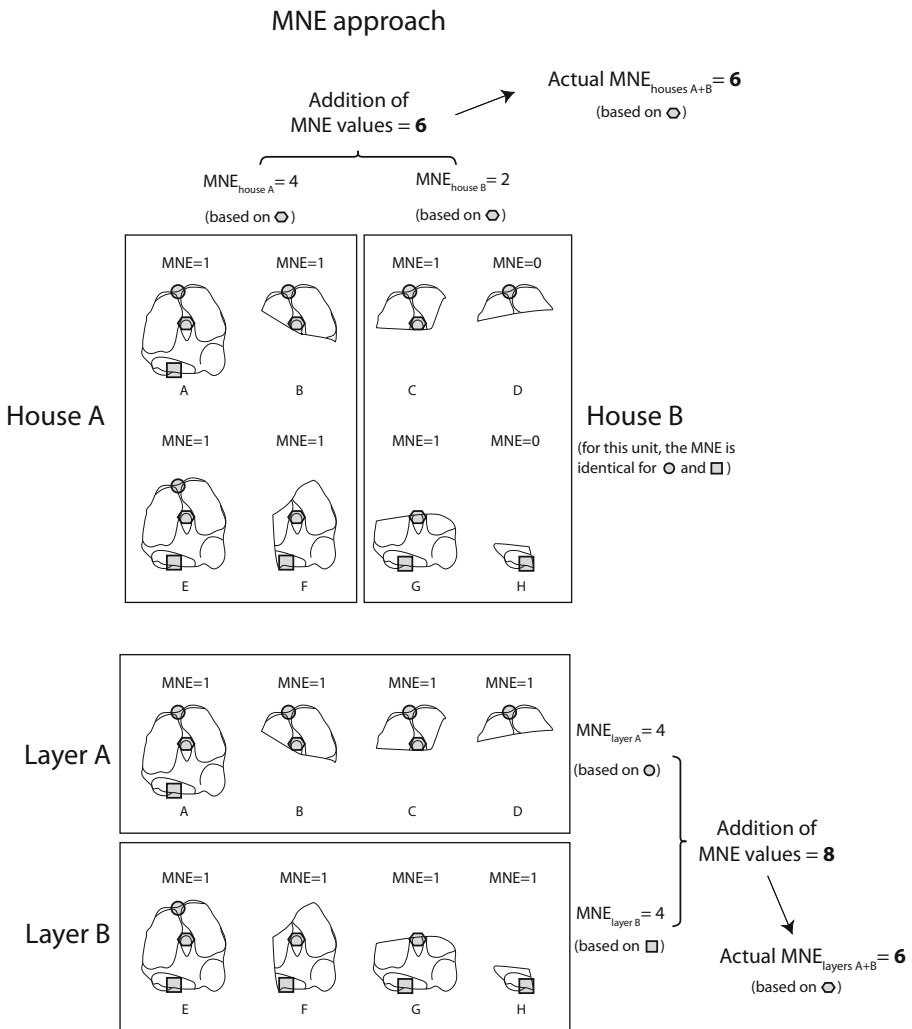


Fig. 14 Example showing how MNE values for the same set of bones differ in two hypothetical situations: a floor plan with two houses and a stratigraphy comprising two layers. In the uppermost example, the total for the two houses (MNE = 6) is consistent with the actual value (MNE = 6) because the same landmark (marked by a polygon) was used. In the lowermost example, the total (MNE = 8) and the actual value (MNE = 6) conflict because different landmarks were used in the derivation of the tallies

metrics such as NISP/MNE ratios—or their converse, MNE/NISP ratios—are unlikely to be reliable proxies of fragmentation because they measure, among other factors, the size of the NISP sample. In fact, any ratio that incorporates a proxy estimate based on the minimum number concept will be affected by this problem, given that built into this approach is a pattern of declining probability of identification of new units with increasing NISP (Lyman 2008). Viable alternatives for the study of fragmentation include the use of mean fragment length and mean area measurements of specimens

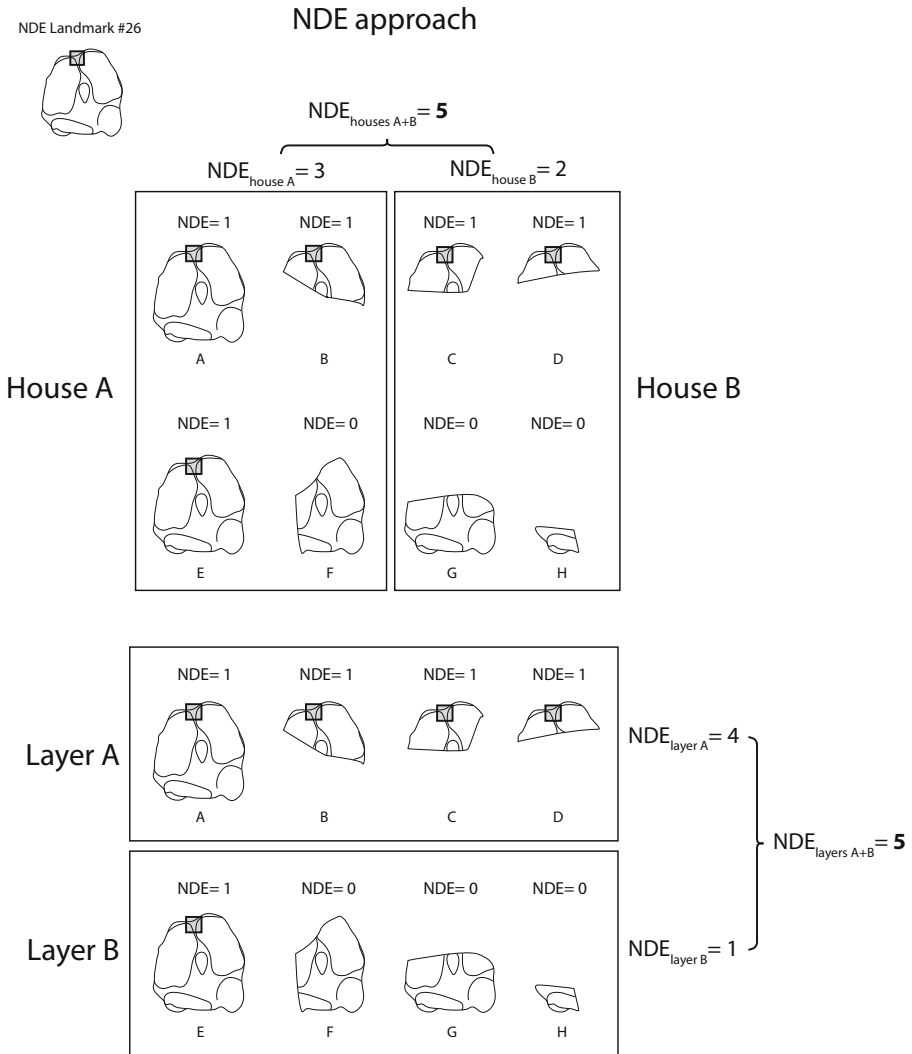


Fig. 15 Two examples involving the same set of bones and the same methods of aggregation shown in Fig. 14, but this time calculated with the NDE. Note that the values derived in the two examples are consistent

(Lyman and O’Brien 1987, pp. 494–497; Morin 2012, pp. 95–98; Cannon 2013, pp. 413–416).

Problems identified in the preceding analyses led to the suggestion of a substitute counting method, the NDE. Like Watson’s (1979) diagnostic zone approach, the NDE is a simpler and more productive alternative to metrics commonly used in archaeozoological analysis. Indeed, unlike MNE, NDE should increase linearly with NISP size and is not affected by the problem of aggregation. Moreover, NDE is additive; counts can be derived and re-derived almost instantaneously as new identifications are entered into a database. Furthermore,

comparisons can more readily be made with mollusk NRE-based MNI counts. These advantages mean that NDE values are more appropriate for statistical treatment than values generated with other approaches such as MNE or MNI. Importantly, in order to facilitate intra- and inter-site comparisons, we encourage archaeozoologists to publish raw NDE data for *all* observed landmarks. Systematic reporting is essential in the present case as it permits analysts to calculate and recalculate NDE values for whole elements using any landmark.

One may object that the NDE approach gives values that tend to be slightly smaller than MNE, and that an element known to be present in the sample may become analytically absent if its specimens show only NDE landmarks <50 % or none at all. These observations are correct and echo points made in the archaeomalacological literature about some of the NRE-based methods of calculation (Mason *et al.* 1998, 2000; Giovas 2009; Gutiérrez Zugasti 2011; Harris *et al.* 2015; Thomas and Mannino 2016). However, generating large (or larger) values is not a guarantee of accuracy, NISP being a clear example. In fact, as pointed out by Ducos (1968) nearly 50 years ago, what is critical is not the magnitude of the values but *their proportionality to the actual number of elements, individuals and species in a sample*. The experimental results seem to confirm that NDE provide estimates that are proportional to known abundances.

In a related vein, it should be noted that attempts to increase MNE (or MNI) tallies through matching do *not* increase accuracy because the success of this exercise is highly dependent on the characteristics and, perhaps more importantly, the size of the sample (Watson 1979; Klein and Cruz-Uribe 1984; Lyman 2006). Indeed, identifying individuals or elements using sex, age, size, and similar criteria is easy with three specimens, a bit more challenging with 10 fragments and becomes complicated with 20 or more remains. Furthermore, matching teeth is much easier than matching long bone shaft specimens or scapula fragments, which introduces another source of bias. Consequently, trying to derive the largest MNE or MNI from a sample in order to get closer to the “real” abundances is a trap because this procedure exaggerates the curvilinear relationship between MNE and NISP. For this reason, we believe this practice should be discontinued.

For similar reasons, and despite relatively encouraging experimental results (Hudson 1990; Domínguez-Rodrigo 2012), MNI is probably a poor proxy measure of taxonomic abundance. Indeed, its curvilinear relationship to NISP is known to influence the representation of rare taxa in small samples, an issue of particular relevance in geographical regions such as the tropics, where collections frequently comprise a wide range of species represented by few specimens (see Emery [2008] and Boileau [2014] for examples). Another problem with this measure is the considerable variation in the way MNI counts are generated between analysts (Payne 1972; Watson 1979; Grayson 1984; Lyman 2008; Reitz and Wing 2008). Although rarely used with the aim of quantifying taxonomic composition, the experimental samples show that Σ MNE (see part I) and Σ NDE counts produce more accurate estimates of species representation than NISP. Indeed, summing element counts by taxon seems a more effective way of interpreting variation in taxonomic composition than counting numbers of specimens or minimum numbers of individuals.

Because they have fewer limitations, the NDE approach and its derivatives (Σ NDE or Σ NNDE depending on whether the values need to be normed) seem to represent improved alternatives relative to MNE and MNI. However, the NDE was not designed

to replace NISP, a more fundamental measure. Given that these last two metrics are partly complementary, more robust interpretations of skeletal and taxonomic abundances can potentially be achieved by using them in concert.

Conclusion

The MNE approach has often been reviewed with mixed enthusiasm, in large part due to the many problems that have been identified with it. Foremost among these are a lack of standardization in calculation methods and the non-additivity of the values. Moreover, our results show that the MNE approach inflates the abundance of rare elements, particularly at small sample sizes. The non-linear relationship with NISP sample size means that MNE is a less than ideal measure of abundance.

The NDE emerges as an improvement over the MNE approach because it largely avoids these problems. In addition to yielding positive experimental results, this metric produces mutually independent values that are presumably unbiased by sample size and methods of aggregation. Moreover, by eliminating the complicated step of comparing and/or drawing specimens to identify zones of overlap, the NDE approach provides gains in time that are significant, particularly in large assemblages. Thus, the NDE approach represents a step forward toward the production of more robust interpretations of past skeletal and taxonomic abundances.

Compliance with Ethical Standards

Conflict of Interest The authors declare that they have no conflict of interest.

Appendix

Table 7 NDE values derived for the MCE and BGRE (Marrow Cracking Experiment and Bone Grease Rendering Experiment, see Morin et al., Part I, this issue)

#	Landmarks	MCE	BGRE	#	Landmarks	MCE	BGRE
	Red deer	NDE	NDE			NDE	NDE
	Humerus			41	Atlas (articulatory surface)		
1	Lmk1 (greater tubercle)	23	8	42	(Inter-articulatory notch)		
2	Lmk2 (<i>Tuberositas teres major</i>)	17	14	43	Axis (<i>Dens axis</i>)		
3	Lmk3 (foramen)	16	17	44	(Articulatory surface)		
4	Lmk4 (fossa of the <i>Capitulum</i>)	16	12	45	Cervical (spinous process)		
	Radius			46	(Articulatory process)		
5	Lmk1 (<i>Tuberositas radii</i>)	19	15	47	Thoracic (artic. surface)		
6	Lmk2 (articulation with the ulna)	15	5	48	(<i>Fovea costalis</i>)		

Table 7 (continued)

#	Landmarks	MCE	BGRE	#	Landmarks	MCE	BGRE
7	Lmk3 (distal ridge)	19	2	49	Lumbar (artic. surface)		
8	Lmk4 (radial styloid process)	21	12	50	(Transverse process)		
	Ulna			51	Sacrum (centrum)		
9	Lmk1 (olecranon)	13	11	52	(Spinous process)		
10	Lmk2 (trochlear notch)	17	15	53	Caudal vertebrae (centrum)		
11	Lmk3 (lat. coronoid process)	17	7	54	Rib (proximal end)	2	
12	Lmk4 (ulnar styloid process)	19	16	55	(Distal end)	1	1
	Metacarpal			56	Sternebrae (>50 %)		
13	Lmk1 (articulatory surface)	23	18	57	Scapula (glenoid cavity)	4	
14	Lmk2 (proximal anterior groove)	23	19	58	(Base of the acromion)	4	1
15	Lmk3 (distal metacarpal canal)	26	16	59	(Axillary border)	3	
16	Lmk4 (fossa condyles/2)	26			Carpals		
17	Lmk 5 (length measurement)			60	Scaphoid	2	1
	Femur			61	Lunatum	2	1
18	Lmk1 (<i>Fovea capitis</i>)	20	19	62	Triquetrum	1	2
19	Lmk2 (foramen)	14	11	63	Pisiform	2	1
20	Lmk3 (<i>Fossa supracondylaris</i>)	17	13	64	Capitatum	2	1
21	Lmk4 (lateral condyle)	15	20	65	Hamatum	2	1
	Tibia			66	Coxal (foramen, ilium)		2
22	Lmk1 (<i>Sulcus extensorius</i>)	19	8	67	(Acetabulum: ischium)	2	
23	Lmk2 (foramen)	16	17	68	(Acetabulum: pubis)	1	
24	Lmk3 (posterior ridge)	16	8	69	Patella (anterior, central)		
25	Lmk4 (medial malleolus)	16	18	70	(Posterior, apex)		
	Metatarsal			71	Malleolus (artic. surface)	6	4
26	Lmk1 (articulatory surface)	22	18		Tarsals		
27	Lmk2 (proximal anterior groove)	21	18	72	Talus (lateral surface)	2	1
28	Lmk3 (distal anterior groove)	15	11	73	(Medial surface)	1	2
29	Lmk4 (fossa condyles/2)	14	0.5	74	Calcaneus (<i>Tuber calcanei</i>)	2	1
30	Lmk 5 (length measurement)			75	(Articulatory surface)	1	2
	Indeterminate metapodial			76	(Distal extremity)	1	2
31	(fossa condyles/2)		38.5	77	Cubo-navicular	1	
	Other bones			78	Smaller cuneiform	2	2
32	Antler (base)			79	Greater cuneiform	2	2
33	Cranium (UD4 + worn UM3)/2			80	Phalanx 1	2	1
34	(petrosal)/2			81	Phalanx 2	1	3
35	Mandible (LD4 + worn LM3)	1	2	82	Phalanx 3	2	1
36	(<i>Foramen mentale</i>)	2	1	83	Vestigial phalanx 1		
37	(Mandibular condyle)		2	84	Vestigial phalanx 2		
38	Hyoid (stylohyoideum)	2	1	85	Vestigial phalanx 3		
39	(Epihyoideum)			86	Vestigial metapodial	46	40
40	(Basihyoideum)			87	Sesamoids		

Table 7 (continued)

#	Landmarks	MCE	BGRE	#	Landmarks	MCE	BGRE
	Cattle						
	Femur						
18	Lmk1 (<i>Fovea capitis</i>)		1				
	Tibia						
23	Lmk2 (foramen)	1					
25	Lmk4 (medial malleolus)		1				
71	Malleolus (artic. surface)	1					

The Σ NDE values for red deer are 220 (MCE) and 179 (BGRE). For cattle, the Σ NDE values are 2 for both experiments. The Σ NDE values were obtained after summing the highest NDE values obtained for each class of elements

References

- Albarella, U., & Davis, S. J. M. (1996). Mammals and birds from Launceston Castle, Cornwall: decline in status and the rise of agriculture. *Circaea*, 12, 1–156.
- Binford, L. R. (1984). *Faunal remains from Klasies River mouth*. New York: Academic Press.
- Blasco, R. (2011). *La amplitud de la dieta cárnica en el Pleistoceno medio peninsular: Una aproximación a partir de la Cova del Bolomor (Tavernes de la Valldigna, Valencia) y del subnivel TD10-1 de Gran Dolina (Sierra de Atapuerca, Burgos)*. Unpublished Ph.D. dissertation, Universitat Rovira I Virgili, Tarragona.
- Boileau, A. (2014). *Maya exploitation of animal resources during the Middle Preclassic period: an archaeozoological analysis from Pacbitun, Belize*. M.A thesis, Peterborough: Trent University.
- Broughton, J. (2004). Prehistoric impacts on California birds: evidence from the Emeryville Shellmound avifauna. *Ornithological Monographs*, 56.
- Bunn, H. T. (1991). A taphonomic perspective on the archaeology of human origins. *Annual Review of Anthropology*, 20, 433–467.
- Bunn, H. T., & Kroll, E. M. (1986). Systematic butchery by Plio/Pleistocene hominids at Olduvai Gorge, Tanzania. *Current Anthropology*, 27, 431–452.
- Cannon, M. D. (2013). NISP, bone fragmentation, and the measurement of taxonomic abundance. *Journal of Archaeological Method and Theory*, 20, 397–419.
- Casteel, R. W. (1977). A consideration of the behavior of the minimum number of individuals index: a problem in faunal characterization. *OSSA*, 3/4, 14–151.
- Castel, J. C. (1999). *Comportements de subsistance au Solutréen et au Badegoulien d'après les faunes de Combe-Saunière (Dordogne) et du Cuzoul de Vers (Lot)*. Unpublished Ph.D. dissertation, Bordeaux: Université de Bordeaux I.
- Castel, J. C. (2011). Archéozoologie de l'Aurignacien de l'Abri Castanet (Sergeac, Dordogne, France): Les fouilles 1994–1998. *Revue de Paléobiologie*, 30, 783–815.
- Chase, P. G. (1999). Bison in the context of complex utilization of faunal resources: a preliminary report on the Mousterian zooarchaeology of La Quina (Charente, France). In J.-P. Brugal, F. David, J. G. Enloe, & J. Jaubert (Eds.), *Le bison: Gibier et moyen de subsistance des hommes du Paléolithique aux Paléindiens des grandes plaines* (pp. 159–184). Antibes: Éditions ADPCA.
- Cho, T.-S. (1998). *Étude archéozoologique de la faune du Périgordien supérieur: couches 2, 3, et 4 de l'abri Pataud, Les Eyzies, Dordogne: Paléoécologie, taphonomie, paléoeconomie*. Unpublished Ph.D. dissertation, Paris: Muséum National d'Histoire Naturelle.
- Claassen, C. (1998). *Shells*. Cambridge: Cambridge University Press.
- Cleghorn, N., & Marean, C. W. (2004). Distinguishing selective transport and *in situ* attrition: a critical review of analytical approaches. *Journal of Taphonomy*, 2, 43–67.

- Costamagno, S. (1999). *Stratégies de chasse et fonction des sites au Magdalénien dans le sud de la France*. Unpublished Ph.D. dissertation, Université de Bordeaux I.
- David, F., & Poulain, T. (2002). Les mammifères (herbivores, carnivores, petits mammifères). In B. Schmider (Ed.), *L'Aurignacien de la Grotte du Renne. Les fouilles d'André Leroi-Gourhan à Arcy-sur-Cure (Yonne)* (pp. 49–95). Paris: Éditions CNRS.
- David, F., Connet, N., Girard, M., Miskovsky, J.-C., Mourer-Chauviré, C., & Roblin-Jouve, A. (2005). Les niveaux du Paléolithique supérieur à la grotte du Bison (Arcy-sur-Cure, Yonne) couches a à d. *Revue Archéologique de l'Est*, 54, 5–50.
- Davis, S. J. M. (1992). *A rapid method for recording information about mammal bones from archaeological sites*. London, English Heritage AML report 19/92.
- Domínguez-Rodrigo, M. (2012). Critical review of the MNI (minimum number of individuals) as a zooarchaeological unit of quantification. *Archaeological and Anthropological Sciences*, 4, 47–59.
- Ducos, P. (1968). *L'origine des animaux domestiques en Palestine. Publications de l'Institut de Préhistoire de l'Université de Bordeaux: Mémoire no. 6*. Bordeaux: Imprimerie Delmas.
- Emery, K. F. (2008). A zooarchaeological test for dietary resource depression at the end of the Classic period in the Petexbatun. *Human Ecology*, 36, 617–634.
- Enloe, J. G. (1993). Subsistence organization in the early Upper Paleolithic: reindeer hunters of the Abri du flageolet. In H. Knecht, A. Pike-Tay, & R. White (Eds.), *Before Lascaux: the complex record of the early Upper Paleolithic* (pp. 101–115). Boca Raton: CRC Press.
- Fernández-Laso, M. C. (2010). *Remontajes de restos faunísticos y relaciones entre áreas domésticas en los niveles K, L y M del Abric Romani (Capellades, Barcelona, España)*. Unpublished Ph.D. dissertation, Tarragona: Universitat Rovira i Virgili.
- Fiore, I., & Tagliacozzo, A. (2008). Oltre lo stambecco: Gli altri mammiferi della struttura abitativa dell'US 26c a Riparo Dalmeri (Trento). *Preistoria Alpina*, 43, 209–236.
- Gerbe, M. (2010). *Économie alimentaire et environnement en Quercy au Paléolithique. Étude des associations fauniques de la séquence des Fieux (Lot)*. Unpublished Ph.D. dissertation, Université d'Aix-Marseille.
- Giovas, C. M. (2009). The shell game: analytic problems in archaeological mollusc quantification. *Journal of Archaeological Science*, 36, 1557–1564.
- Grayson, D. K. (1973). On the methodology of faunal analysis. *American Antiquity*, 38, 432–439.
- Grayson, D. K. (1978a). Minimum numbers and sample size in vertebrate faunal analysis. *American Antiquity*, 43, 53–65.
- Grayson, D. K. (1978b). Reconstructing mammalian communities: a discussion of Shotwell's method of paleoecological analysis. *Paleobiology*, 4, 77–81.
- Grayson, D. K. (1979). On the quantification of vertebrate archaeofaunas. *Advances in Archaeological Method and Theory*, 2, 199–237.
- Grayson, D. K. (1984). *Quantitative zooarchaeology: topics in the analysis of archaeological faunas*. Orlando: Academic Press.
- Grayson, D. K., & Frey, C. J. (2004). Measuring skeletal representation. *Journal of Taphonomy*, 2, 27–42.
- Gutiérrez Zugasti, F. I. (2011). Shell fragmentation as a tool for quantification and identification of taphonomic processes in archaeomalacological analysis: the case of the Cantabrian region (northern Spain). *Archaeometry*, 53, 614–630.
- Harris, M., Weisler, M., & Faulkner, P. (2015). A refined protocol for calculating MNI in archaeological molluscan shell assemblages: a Marshall Islands case study. *Journal of Archaeological Science*, 57, 168–179.
- Haws, J. A. (2003). *An investigation of late Upper Paleolithic and Epipaleolithic hunter-gatherer subsistence and settlement patterns in Central Portugal*. Unpublished Ph.D. dissertation, University of Wisconsin-Madison.
- Hudson, J. 1990. *Advancing methods in zooarchaeology: an ethnoarchaeological study among the Aka Pygmies*. Unpublished Ph.D. dissertation, Santa Barbara: University of California.
- Klein, R. G., & Cruz-Urbe, K. (1984). *The analysis of animal bones from archaeological sites*. Chicago: University of Chicago Press.
- Klein, R. G., Cruz-Urbe, K., & Milo, R. G. (1999). Skeletal part representation in archaeofaunas: comments on “explaining the ‘Klasies pattern’: Kua ethnoarchaeology, the Die Kelders middle stone age archaeofauna, long bone fragmentation and carnivore ravaging” by Bartram & Marean. *Journal of Archaeological Science*, 26, 1225–1234.
- Kuntz, D. (2006). Données nouvelles sur les stratégies d'acquisition et de traitement des carcasses au cours du Magdalénien supérieur dans la vallée de l'Aveyron: L'exemple de La Magdeleine La Plaine (Penne, Tam). *Préhistoire du Sud-Ouest*, 13, 151–166.
- Lyman, R. L. (1994). *Vertebrate taphonomy*. New York: Cambridge University Press.
- Lyman, R. L. (2003). Quantification and sampling of faunal remains in owl pellets. *Journal of Taphonomy*, 1, 3–14.

- Lyman, R. L. (2006). Identifying bilateral pairs of deer (*Odocoileus* sp.) bones: how symmetrical is symmetrical enough? *Journal of Archaeological Science*, *33*, 1237–1255.
- Lyman, R. L. (2008). *Quantitative paleozoology*. New York: Cambridge University Press.
- Lyman, R. L., & O'Brien, M. J. (1987). Plow-zone zooarchaeology: fragmentation and identifiability. *Journal of Field Archaeology*, *14*, 493–498.
- Magniez, P. (2010). *Étude paléontologique des artiodactyles de la grotte Tournal (Bize-Minervois, Aude, France): Étude taphonomique, archéozoologique et paléocéologique des grands mammifères dans leur cadre biostratigraphique et paléoenvironnemental*. Unpublished Ph.D. dissertation, Perpignan: Université Via Domitia.
- Marean, C. W., & Kim, S. Y. (1998). Mousterian large-mammal remains from Kobeh cave: behavioral implications for Neanderthals and early modern humans. *Current Anthropology*, *39*, 79–113.
- Marean, C. W., Abe, Y., Nilssen, P. J., & Stone, E. C. (2001). Estimating the minimum number of skeletal elements (MNE) in zooarchaeology: a review and a new image-analysis GIS approach. *American Antiquity*, *66*, 333–348.
- Marín Arroyo, A. B. (2009). A comparative study of analytic profile interpretation at El Mirón cave (Cantabria, Spain). *Archaeofauna*, *18*, 79–98.
- Mason, R. D., Peterson, M. L., & Tiffany, J. A. (1998). Weighing vs. counting: measurement reliability and the California school of midden analysis. *American Antiquity*, *63*, 303–324.
- Mason, R. D., Peterson, M. L., & Tiffany, J. A. (2000). Weighing and counting shell: a response to Glassow and Claassen. *American Antiquity*, *65*, 757–761.
- Morin, E. (2012). *Reassessing Paleolithic subsistence: the Neanderthal and modern human foragers of Saint-Césaire, France*. Cambridge: Cambridge University Press.
- Niven, L., Steele, T. E., Rendu, W., Mallye, J.-B., McPherron, S. P., et al. (2012). Neanderthal mobility and large-game hunting: the exploitation of reindeer during the Quina Mousterian at Chez-Pinaud Jonzac (Charente-Maritime, France). *Journal of Human Evolution*, *63*, 624–635.
- Payne, S. (1972). On the interpretation of bone samples from archaeological sites. In E. S. Higgs (Ed.), *Papers in economic prehistory* (pp. 65–81). Cambridge: Cambridge University Press.
- Pickering, T. R., Marean, C. W., & Dominguez-Rodrigo, M. (2003). Importance of limb bone shaft fragments in zooarchaeology: a response to "on *in situ* attrition and vertebrate body part profiles" (2002) by M.C. Stiner. *Journal of Archaeological Science*, *30*, 1469–1482.
- Psathi, E. (2003). *Les sites moustériens de la Caverna delle Fate et de l'Arma delle Manie (Ligurie, Italie). Étude paléontologique et archéozoologique des faunes des grands mammifères*. Unpublished Ph.D. dissertation, Paris: Muséum National d'Histoire Naturelle.
- Reitz, E. J., & Wing, E. S. (2008). *Zooarchaeology* (Second ed.). Cambridge: Cambridge University Press.
- Romandini, M., Nannini, N., Tagliacozzo, A., & Peresani, M. (2014). The ungulate assemblage from layer A9 at Grotta di Fumane, Italy: a zooarchaeological contribution to the reconstruction of Neanderthal ecology. *Quaternary International*, *337*, 11–27.
- Rosell, J. (2001). *Patrons d'aprofitament de les biomasses animals durant el Pleistocè inferior i mig (Sierra de Atapuerca, Burgos) I superior (Abric Romani, Barcelona)*. Unpublished Ph.D. dissertation, Tarragona: Universitat Rovira i Virgili.
- Rosell, J., Blasco, R., Rivals, F., Chacón, M. G., Menéndez, L., Morales, J. I., Rodríguez, A., Cebrià, A., Carbonell, E., & Serrat, D. (2010). A stop along the way: the role of Neanderthal groups at level III of Teixoneres cave (Moià, Barcelona, Spain). *Quaternaire*, *21*(2), 139–154.
- Soulier, M.-C. (2013). *Entre alimentaire et technique: L'exploitation animale aux débuts du Paléolithique supérieur. Stratégies de subsistance et chaînes opératoires de traitement du gibier à Isturitz, La Quina aval, Roc-de-Combe et Les Abeilles*. Unpublished Ph.D. dissertation, Université de Toulouse.
- Stiner, M. C. (2002). On *in situ* attrition and vertebrate body part profiles. *Journal of Archaeological Science*, *29*, 979–991.
- Surmély, F., Fontana, L., Bourdelle, Y., & Liabeuf, R. (1997). Nouveaux éléments apportés à l'étude du site magdalénien d'Enval (Vic-le-Comte, Puy-de-Dôme, France) et du peuplement de la Limagne d'Auvergne. *Bulletin de la Société Préhistorique Française*, *94*, 172–181.
- Thomas, K. D., & Mannino, M. A. (2016). Making numbers count: beyond minimum numbers of individuals (MNI) for the quantification of mollusc assemblages from shell matrix sites. *Quaternary International*, in press.
- Tolmie, C. (2013). *Animals for food, animals for tools: fauna as a source of raw material at Abri Cellier, Dordogne, and the Grotte du Renne, Arcy-sur-Cure*. Unpublished Ph.D. dissertation, University of Iowa.

- Valensi, P., Crégut-Bonnoure, E., & Defleur, A. (2012). Archaeozoological data from the Mousterian level from Moula-Guercy (Ardèche, France) bearing cannibalised Neanderthal remains. *Quaternary International*, 252, 48–55.
- Valensi, P., Michel, V., El Guennouni, K., & Liouville, M. (2013). New data on human behavior from a 160,000 year old Acheulean occupation level at Lazaret cave, south-East France: an archaeozoological approach. *Quaternary International*, 316, 123–139.
- Watson, J. P. N. (1979). The estimation of the relative frequencies of mammalian species: Khirokitia 1972. *Journal of Archaeological Science*, 6, 127–137.